Studies on the Redox State of Metal Ions in Glass and the Basic Properties of Glass Melts

Masaru Yamashita

SEPTEMBER 2008

Studies on the Redox State of Metal Ions in Glass and the Basic Properties of Glass Melts

A dissertation submitted to

THE GRADUATE SCHOOL OF ENGINEERING SCIENCE

OSAKA UNIVERSITY

in partial fulfillment of the requirements for the degree of

DOCTOR OF PHILOSOPHY IN ENGINEERING

BY

Masaru Yamashita

SEPTEMBER 2008

Chapter 1 General Introduction

1-1 Background and history of the study of oxide melts

1-1.1 *Previous studies of oxide melts*

Studies of the properties of oxide melts and glass have been conducted since the 19th century, and such properties as viscosity have been studied in detail. Among the oxide melts, slag has been most extensively studied. These properties are especially important for metal production, since slag is produced during metal smelting. Molten rocks have also been studied, as they are important for geological mineralogy. Measurement of the properties of melts is not easy due to the high temperature conditions, normally above 1200 ^{o}C, which limit the materials to be used as probes, and to their structure. However, since the melt properties of steel slag are important to steel production, methods for measuring the properties at high temperatures have been developed.

Slag consists primarily of SiO_2, CaO, and Al_2O_3. The main difference between ordinary silicate glasses and slag is the amounts of silica and alkali oxides included in them. The glass used for windows and bottles usually contains more than 70 mol% of silica and 12 to 15 mol% of Na_2O. In contrast, slag contains less silica, more CaO, and no Na_2O. This difference in composition results in the difference in viscosity at high temperatures. Though the softening temperature of ordinary glass is lower than that of slag, the viscosity at higher temperatures is higher in ordinary glass than in slag. Another feature of glass melt is its corrosivity, which arises from the high Na_2O content. Because of the corrosivity and high temperature of glass melt, the container of the melt is easily deteriorated unless platinum is used as the container. This problem has limited the study of glass melts, and most of the previous work has been carried out on borate glasses, which have low viscosity even below 1000 ^{o}C. Furthermore, the data for ordinary silicate glasses have been limited to such properties as viscosity.

1-1.2 *Electrochemical measurement of oxide melt*

In the fields of slag and molten rocks, studies have focused on the thermodynamical properties such as the formation energy, the phase diagram and activity of oxide ion, and the bonding structure. The free energy change has been evaluated based on the measurements of equilibrium change with temperature and on direct measurements of the reaction heat with a calorimeter. These methods are, however, not suitable for glass melt since the melt is a mixture of many oxides and has no phase transformation. Alternatively, the free energy change can be measured electrochemically. The electrochemical method is popular in the field of molten salt. In oxide glass melt, however, use of this method has not been common because higher temperatures are needed for glass melt than for molten salt. In addition, the liquid-junction potential may not be ignored. However, in 1972, Sato et al. succeeded in measuring the Na_2O activity in borate glass melts[1] using two stabilized zirconia electrodes that transmit oxide ions at high temperature. They measured the activity of the oxide ion in several series of compositions such as Na_2O-B_2O_3,[1,2] Na_2O-SiO_2,[3] and Na_2O-GeO_2.[4] They determined not only the equilibrium of the main component, but also the equilibrium of additives by the electrochemical method.

The redox state for polyvalent ions is also an important property in glass melt. Slag contains polyvalent ions, M^{m+}, formed from metals such as Fe. The redox state of M is represented by the equation,

$$M^{m+} + (n/4)O_2 \rightarrow M^{(m+n)+} + (n/2)O^{2-} \qquad (1).$$

Since this equation contains oxide ion and oxygen, the redox equilibrium depends on the activity of the oxide ion and the concentrations of oxygen in the melt. Oxygen activity in slag melt was measured by Goto et al. in 1968.[5] They used a stabilized zirconia electrode[6] as a reference electrode. The oxygen activity was calculated using

the Nernst equation on the basis of the voltage difference between a metal probe outside the zirconia in the melt and an electrode wire inside the zirconia. Oxygen activity in slag tends to be very low since the slag is reduced by contacting to molten metal. Hence metal/metal oxides such as Mo/MoO_2 are used as a reference instead of air in the zirconia electrode, and the oxygen activity is determined from the equilibrium of the metal/metal oxide. The oxygen activities in glass melts have been measured since 1980.[7] In the present case, air was used for the reference gas since the oxygen activity is higher in glass melt than in slag. From measurements of oxygen activities in glass melt, it has been clarified that the activity value changes with temperature and that the degree of change depends on the polyvalent ions. When As or Sb is included in the glass melt as a refining agent, the oxygen activity changes with temperature. The redox potential of polyvalent ion M can be measured by voltammetry, and the measurements have been carried out for many ions such as Cr, Mn, Fe, Cu, As, Sb, and Ce, in many systems. For the measurements, cyclic voltammetry was at first used by Sasahira and Yokokawa.[8] Recently, differential pulse voltammetry such as square wave voltammetry[9] has been used, as this method is advantageous in eliminating the effect of the capacitance and can accurately determine the redox potential. By this method, we can determine the redox ratio of a polyvalent ion contained in melt if we know the oxygen activity in the melt and the redox potential of the ion.

1-1.3 *Importance of the measurement of melt properties*

The measurement of melt properties is important not only scientifically but also practically. In the glass production process, raw materials such as carbonates are first decomposed and react with other materials such as silica. Melt is then generated, and bubbles are formed inside the melt. In order to produce high-quality homogeneous

glass without bubbles or striae, information about the properties of glass melts is important. Hence, the properties of glass melts have long been studied. Multivalent ions are often added to the raw material. If multivalent ions are present in the melt as a refining agent, oxygen activity increases with increasing temperature and the generated oxygen enters into the bubbles and helps them to rise to the surface. When temperature decreases, oxygen activity decreases and the residual oxygen bubbles are absorbed in the melt.

Recently, computer simulation of glass melting has become a useful tool for calculation of melt flow in the furnace. In such a simulation, accurate parameters are needed for precise calculations; in particular, viscosity, density, surface tension, thermal conductivity, infrared transmittance, etc. are important. Gas solubility, oxygen activity and diffusion, redox reactions, etc., are also important properties for the simulation of bubble formation and shrinkage. To meet such these research needs, the New Glass Forum Japan supported a study of glass-melt properties.[10] In this project, the methods for measuring density, surface tension, thermal conductivity, electric conductivity, and X-ray diffraction patterns of glass melt at high temperatures were investigated. The necessity for obtaining accurate surface-tension values was also shown in the study of the glass-flow simulation carried out by NEDO. As a part of this study, the expansion and shrinkage of rising bubbles in the melt was simulated by Yoshikawa et al.[11] In the equation used for the simulation, parameters such as surface tension, gas solubility, and the reaction between oxygen and redox species were included.

1-2 The objectives of this thesis work

1-2.1 *Electrochemical measurement of oxygen activity in glass melt*

Since oxygen activity in glass melt is directly related to the redox ratio of the

polyvalent ions included in it, the oxygen activity can be a useful measure of the ratio. During glass melting from raw materials, the oxygen activity will change with time and the value must be dependent on the melting methods. This activity change during melting has, however, not been studied in detail.

Determination of the oxygen activity as a measure of the oxidation state of redox species in glass is one of the chief motivation of this thesis work. The experimental methods for measuring oxygen activity in glass melt are described and a theoretical explanation is provided in chapter 2. The oxygen activity change was determined experimentally during the melting process, and the resultant oxidation state of redox species in glass is explained in chapter 3.

The oxidation state of redox species is also affected by the diffusion process of oxygen in glass melt. In order to obtain the necessary information, oxygen diffusion has been measured by tracer diffusion[12] and activity change.[13] The first method uses an isotope such as ^{17}O or ^{18}O, and its penetration depth in glass is determined by mass analysis. This method can measure the diffusion coefficient of total oxygen element, which includes oxygen atoms, oxygen molecules, oxide ions, and oxygen atoms bonded to other elements. However, the diffusion coefficients of these species must be different. Although the diffusion coefficients of oxygen atoms or molecules are high in glass melt, their contribution to the value determined by the method is small due to the small amounts of these species included in the glass melt. The second method can trace the diffusion of oxygen atoms or molecules by monitoring their activities in the glass melt. However, reliable data have not been reported by this method, probably due to experimental problems. To solve these problems, the author used a probe lead that was totally covered with an insulating material and succeeded in determining the oxygen diffusion coefficient in glass melt. The method for measuring the oxygen diffusion

coefficient is explained and the results are reported in chapter 4. If redox ions are included in the melt, they will work as buffers for the change of oxygen activity because they react with oxide or oxygen atoms or molecules. The effects of these species are also discussed in the chapter.

1-2.2 *Surface tension of glass melt*

The viscosity, density, and surface tension of glass melt have been studied. Of these properties, viscosity has been measured extensively and accurate values have been obtained by several methods. Although the accurate measurement is not easy, density of glass melt can be measured by the Archimedes method using a Pt ball.[14] It is also difficult to obtain accurate data regarding the surface tension of glass melt. Since the data are important to the computer simulation of the glass flow, surface tension has been a subject of study in the field of glass science. The surface tension has been measured by the Du Nouy ring method,[15] the maximum bubble pressure method,[16-18] the sessile drop method[19,20] and the pendant drop method.[21] The former two methods are dynamic ones, and the latter two are static. Drop methods that are static may give accurate data if the drop shape is precisely measured. Recent development of CCD imaging and computer calculations has resulted in higher accuracy in the data. However, the shape of the drops used in these methods is affected by the surface wettability and by the volatility of the liquid. In contrast, dynamic methods are easier to perform because they are based on force or pressure, which can be precisely measured. However, the application of these methods to viscous liquids such as glass melts has been difficult because the viscosity requires extra force to expand the surface. Therefore, for their application to glass melt, some corrections must be made in the relationship between the pressure and the bubble-formation rate. A method for correcting the relationship in the

maximum bubble pressure method is presented in chapter 5.

1-2.3 *Solubility of noble metals in glass melt*

The solubility of noble metals in glass melt is another important property in practical applications, and especially in the melting of nuclear waste glass, since the precipitates of Ru and Pd, which are included in the nuclear waste, disturb the Joule's heat melting. Ruthenium is known to precipitate as RuO_2 to form needle-like crystals, which may short-circuit between the electrodes for heating. In order to prevent this short-circuiting, the practical furnace has an inclined bottom wall and the precipitated RuO_2 is pulled from the furnace through the bottom together with molten glass. In order to further prevent the problem, the properties of Ru in glass melt should be clarified. The behavior and solubility of Ru in glass melt is discussed in chapter 6.

References

1. S. Sato, T. Yokokawa, H. Kita and K. Niwa, *J. Electrochem. Soc.*, **119**, 1524 (1972).
2. H. Itoh, A. Sasahira, T. Maekawa and T. Yokokawa, *J. C. S. Faraday Trans. I*, **80**, 473 (1984).
3. S. Kohsaka, S. Sato and T. Yokokawa, *J. Chem. Thermodynamics*, **11**, 547 (1979).
4. S. Kohsaka, S. Sato and T. Yokokawa, *J. Chem. Thermodynamics*, **10**, 117 (1978).
5. K. Goto, M. Sasabe and M. Someno, *Trans. TMS-AIME*, **242**, 1757 (1968).
6. K. Kuikkola and C. Wagner, *J. Electrochem. Soc.*, **104**, 379 (1957).
7. T. Tran and M. P. Brungs, *Phys. Chem. Glasses*, **21**, 178-183 (1980).
8. A. Sasahira and T. Yokokawa, *Electrochim. Acta*, **29**, 533 (1984).
9. J. G. Osteryoung and J. J. O'Dea, in: *Electroanalytical Chemistry*, ed. A. J. Bard, Vol. 14, Dekker, New York, (1986) p.209.
10. NEDO Houkokusyo 010019278 (2001).
11. H. Yoshikawa and Y. Kawase, *Glastech. Ber. Glass Sci. Techn.*, **70**(**2**), 31-40 (1997).
12. R. Terai and Y. Oishi, *Glastech. Ber.*, **50**(**4**), 68-73 (1977).
13. J. P. Hilger and O. Lafroukhi, *Glastech. Ber.*, **64**, 299-304 (1991).
14. K. Matsushita, NEDO Houkokusyo 010019278 (2000) p.41.
15. K. Kubota, H. Masuda, S. Fujino and K. Morinaga, *J. Ceram. Soc. Japan*, **106**, 909-913 (1998).
16. A. E. Badger, C. W. Parmelee and A. E. Williams, *J. Am. Ceram. Soc.*, **20**, 325-329 (1937).
17. C. A. Bradley, *J. Am. Ceram. Soc.*, **21**, 339-344 (1938).
18. S. Akhtar and M. Cable, *Glass Technology*, **9**, 145-151 (1968).
19. K. Ghanbari-Ahari, M. Askari and A. M. Cameron, *Phys. Chem. Glasses*, **32**, 72-76

(1991).

20. A. Kucuk, A. G. Clare and L. E. Jones, *Ceram. Trans.*, **82**, 287-298 (1998).

21. A. Yasumori, N. Nakazawa, D. Kawamura, Y. Kameshima and K. Okada, Abstract of 12th fall meeting of the ceramic society of Japan (1999) p.82.

Chapter 2. Measurement of oxygen activity in glass melts

2-1 Introduction

Bubbles in the glass are a major problem in glass production. Since limits on their size and number have become stricter, their removal is an important issue. Bubbles are generated in glass production by the decomposition of raw materials such as carbonate and hydroxide and by air encapsulated in powdery raw materials. They rise to the surface when the melt temperature increases and viscosity becomes low. Bubble generation and shrinkage is related to many other factors such as the gas solubility, viscosity, surface tension and composition of the melt, and atmosphere and temperature. In order to control bubble generation, polyvalent elements such as arsenic or antimony, known as refining agents, are sometimes added to the raw material. At high temperatures, the refining agent converts to its lower valence state and releases oxygen, which enters and expands the bubbles, resulting in their removal from the melt. During cooling, the refining agent reverts to its higher valence state and absorbs the residual oxygen bubbles.[1]

The use of arsenic or antimony is, however, undesirable for environmental reasons[2] and other refining reagents are needed. Sodium sulfate is used as the refining agent in the production of sheet and bottle glass. It decomposes at high temperature and releases oxygen and sulfur dioxide, which assist the removal of bubbles. However, it does not exercise the function of oxygen absorption during cooling. Certain other refining agents are undesirable because they affect the color of the glass.

To resolve the problem, the development of new refining agents is needed. The redox state of polyvalent elements in glass melt is dependent on the redox potential of the element and the oxygen activity in the melt. The redox potential, which is affected by the melt composition and temperature, can be experimentally determined by voltammetry. A solution to the problem also requires a deeper understanding of the

behavior of oxygen in the melt, as this also affects the redox potential. The solubility of oxygen in the melt depends on the glass composition and on temperature and atmosphere. Oxygen activity in the melt can be measured by the electromotive force (EMF) method using a working electrodes and an oxygen reference electrode.[3] For the latter electrode, stabilized zirconia is used.[4]

2-2 Principle for measurement of oxygen activity and redox potential of polyvalent ions

2-2.1 *Oxygen activity*

The configuration of the electrodes for the EMF measurements is shown in Fig. 1. The equilibrium between oxygen and oxide ion is represented as follows

$$1/2O_2 + 2e \rightleftarrows O_2 \quad (1),$$

and obtains in the melt both inside the zirconia electrode and on the platinum electrode. The electrode potentials, $E_{(\mathrm{I})}$ and $E_{(\mathrm{II})}$ for the zirconia and Pt electrodes, are shown as

$$E_{(\mathrm{I})} = E^0 + (\mathrm{R}T/4\mathrm{F}) \ln (pO_2/ (aO^{2-}_{(\mathrm{I})})^2), \quad (2)$$

$$E_{(\mathrm{II})} = E^0 + (\mathrm{R}T/4\mathrm{F}) \ln (aO_2 / (aO^{2-}_{(\mathrm{II})})^2) \quad (3)$$

where pO_2 is the oxygen partial pressure in the zirconia electrode, $aO^{2-}_{(\mathrm{I})}$ is the oxide ion activity in stabilized zirconia, aO_2 and $aO^{2-}_{(\mathrm{II})}$ are the oxygen and oxide ion activities, respectively, on the Pt electrode, R is the gas constant, T is the absolute temperature, and F is the Faraday constant. Since the oxide ion activities are the same at steady state, the potential difference ΔE, namely EMF, is

$$\Delta E = (\mathrm{R}T/4\mathrm{F}) \ln (aO_2 / pO_2) \quad (4).$$

The zirconia electrode can be used as the standard electrode and the potential is 0 V if the oxygen pressure inside the electrode is 1 atm. Thus, from equation (2), we deduce

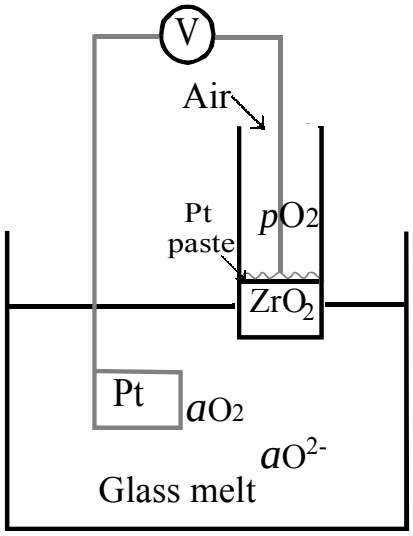

Fig. 1. Illustration of oxygen activity measurement in glass melt. A Pt electrode is immersed in melt with oxygen activity, aO_2, and oxide ion activity, aO^{2-}. A zirconia electrode with reference air is dipped in the melt.

$$0 = E^0 + (RT/2F) \ln (1 / aO^{2-}{}_{(I)}),$$

and

$$E^0 = (RT/2F) \ln (aO^{2-}{}_{(I)}) \quad (5)$$

$$E_{(I)} = (RT/4F) \ln (pO_2) \quad (6).$$

If there is a separator between the electrodes and the activities of oxide and sodium ion in the melt on either side of the separator are different, the potential difference between the two sides of the separator membrane, ΔE_m, is

$$\Delta E_m = (RT/F) \ln (aNa^+{}_{(I)} / aNa^+{}_{(II)})$$

since the transport number of sodium ion is close to unity in glass melt containing soda. The potential difference between the electrodes is

$$\Delta E = (RT/4F) \ln (aO_2 / (aO^{2-}{}_{(II)})^2) - (RT/4F) \ln(pO_2 / (aO^{2-}{}_{(I)})^2) + (RT/F) \ln (aNa^+{}_{(I)} / aNa^+{}_{(II)})$$

$$= (RT/4F) \ln (a O_2 / p O_2) + (RT/2F) \ln (a Na_2O_{(I)} / a Na_2O_{(II)}) \qquad (7).$$

The difference in oxide ion activity between different melt compositions can be measured using this principle.[5]

2-2.2 *Redox potential of polyvalent ions*

When a polyvalent ion such as iron or antimony is contained in a melt, the equilibrium

$$M^{(m+n)+} + ne \rightleftarrows M^{m+} \qquad (8)$$

obtains in the Pt electrode. The potential can be represented by

$$E = E^{0'} + RT/nF \ln ([M^{(m+n)+}]/[M^{m+}]) \qquad (9)$$

if the activity coefficients of both ions are unity. Since $E^{0'}$ cannot be obtained directly from the electrochemical measurement alone, the half-wave potential, $E^{1/2}$, is often used in place of $E^{0'}$. $E^{1/2}$ values are determined by square-wave voltammetry (SWV)[6] and are reported for many ions in glass melts.[7,8] Theoretically, the relationship between $E^{0'}$ and $E^{1/2}$ is written as

$$E^{1/2} = E^{0'} + (RT/nF) \ln (D_M{}^{m+}/D_M{}^{(m+n)+})^{1/2} \qquad (10),[9]$$

where $D_M{}^{(m+n)+}$ and $D_M{}^{m+}$ are the diffusion coefficients for the oxidant and the reductant. Strictly speaking, therefore, the use of $E^{1/2}$ for $E^{0'}$ is valid only when the diffusion coefficients are closely similar.

When redox polyvalent ions are present in melt, they react with oxygen. The reaction is generalized by

$$M^{(m+n)+} + n/2 O^{2-} \rightleftarrows M^{m+} + n/4 O_2 \qquad (11).$$

When the reaction reaches the equilibrium state, the potential of the Pt electrode in the melt is given by both Eqs. (3) and (9), which give the same redox potential. In glass melt, Eq. (11) reaches equilibrium very fast due to the high temperatures. Therefore,

once we know the potential of the Pt electrode (or EMF between the Pt and zirconia electrodes), we can obtain information on the aO_2/pO_2 and $[M^{(m+n)+}]/[M^{m+}]$ ratios using Eqs. (4) and (9).

2-3 Experimental

In the experiment, the base glass composition was chosen to be $70SiO_2$-$20Na_2O$-10CaO. Glass with the base composition was prepared using SiO_2, Na_2CO_3 and $CaCO_3$ as the raw materials. Three kinds of glasses were prepared; (1) base composition, (2) 1 mol% of Sb_2O_3 added as refining agent, and (3) 1 mol% of sulfur component added as refining agent. The glass containing the sulfur component was prepared by substituting 1 mol% of sodium carbonate in the base component with sodium sulfate and sodium sulfide. These materials were mixed thoroughly, melted in a Pt crucible inside an electric furnace at 1400 ^oC, and poured onto graphite plates. The resulting glass samples were then remelted in an alumina crucible (PSA999) inside an electric furnace.

The structure of the zirconia electrode is shown in Fig. 2-(a). Platinum paste was applied to the hollow of an yttria-stabilized zirconia rod and platinum wire attached to the paste as a lead. The rod was then attached to an alumina tube with zirconia cement. Air as a reference gas was passed into the tube through another thin tube of alumina. The Pt electrode, for which a platinum wire of 1 mmϕ was used, was covered except for the tip with an alumina tube with an inner diameter of 1 mmϕ and an outer diameter of 3 mmϕ to serve as an insulator at the melt-air interface, as shown in Fig. 3. Although alumina, as stated in Chapter 4 below, is not a perfect insulating material, the potential can be measured roughly because of the high electric resistivity.

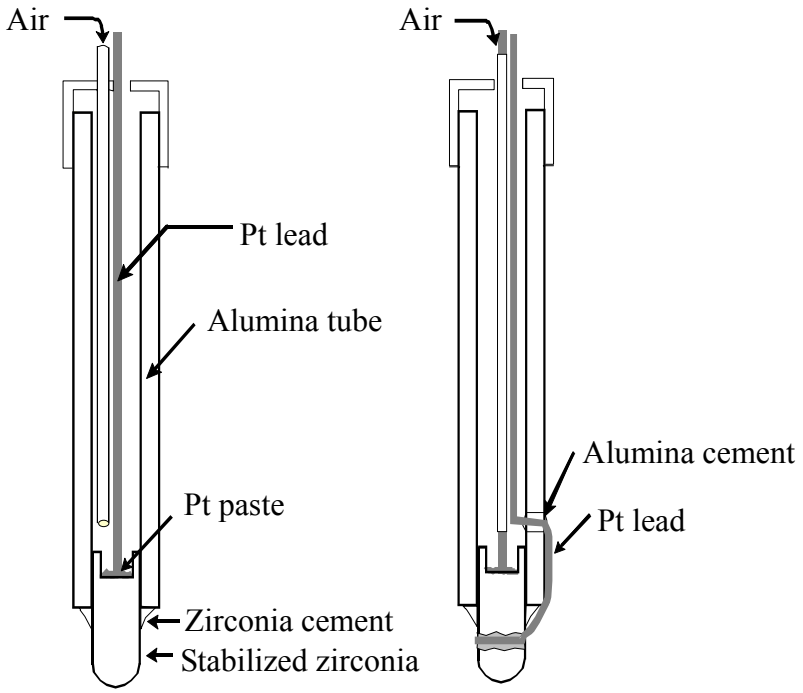

Fig. 2. Structure of zirconia electrode. (a): Standard electrode in glass melt for oxygen activity measurement. (b): Oxygen concentration sensor in atmosphere.

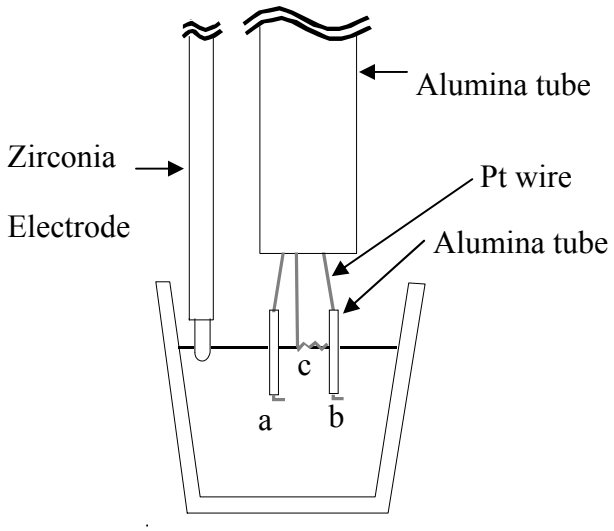

Fig. 3. Configuration of electrodes. a, b: Type I electrode for oxygen activity measurement in bulk, c: Type II electrode for measurement at surface.

EMF between the zirconia and Pt electrodes was measured with a digital voltmeter, as shown in Fig. 1. Oxygen activity was calculated from EMF using equation (4). The value of pO_2 in the equation was 0.21. Air or N_2 gas was passed into the electric furnace, where the oxygen concentration was measured with a zirconia sensor which had an extra platinum wire electrode on the outside of the zirconia electrode mentioned above, as shown in Fig. 2-(b). The oxygen concentration was also measured with an oxygen monitor (Toray Engineering, LC-750L) at the gas outlet of the furnace.

2-4 Result and Discussion

The changes in oxygen activity in glass melt without additives were measured under varying conditions of temperature and atmosphere. The results are shown in Figures 4 and 5. The value at the melt surface, represented by curve no. 3 in Fig. 5, responded quickly to the change in atmosphere. The activity values in curves no.1, 2 and 3 of Fig. 4 differed slightly, which may have been caused by non-uniformity of the melt. When the temperature was varied, oxygen activity changed slightly. Theoretically, in the melt without additives, the activity should not change with temperature, as shown in Fig. 4. The change in the oxygen activity seen in Fig. 5 is probably due to redox ions contained in the melt as contaminants. When the oxygen content in the atmosphere was lowered, oxygen activity in the melt decreased gradually, as seen in Figs. 4 and 5. This was due to oxygen diffusion from the bulk to the surface of the melt.

Figure 6 shows the change in oxygen activity in the soda-lime-silicate melt containing 1 mol% of Sb_2O_3. When the temperature was raised or lowered, the oxygen activity went up or down accordingly. Such changes were caused by a shift in the

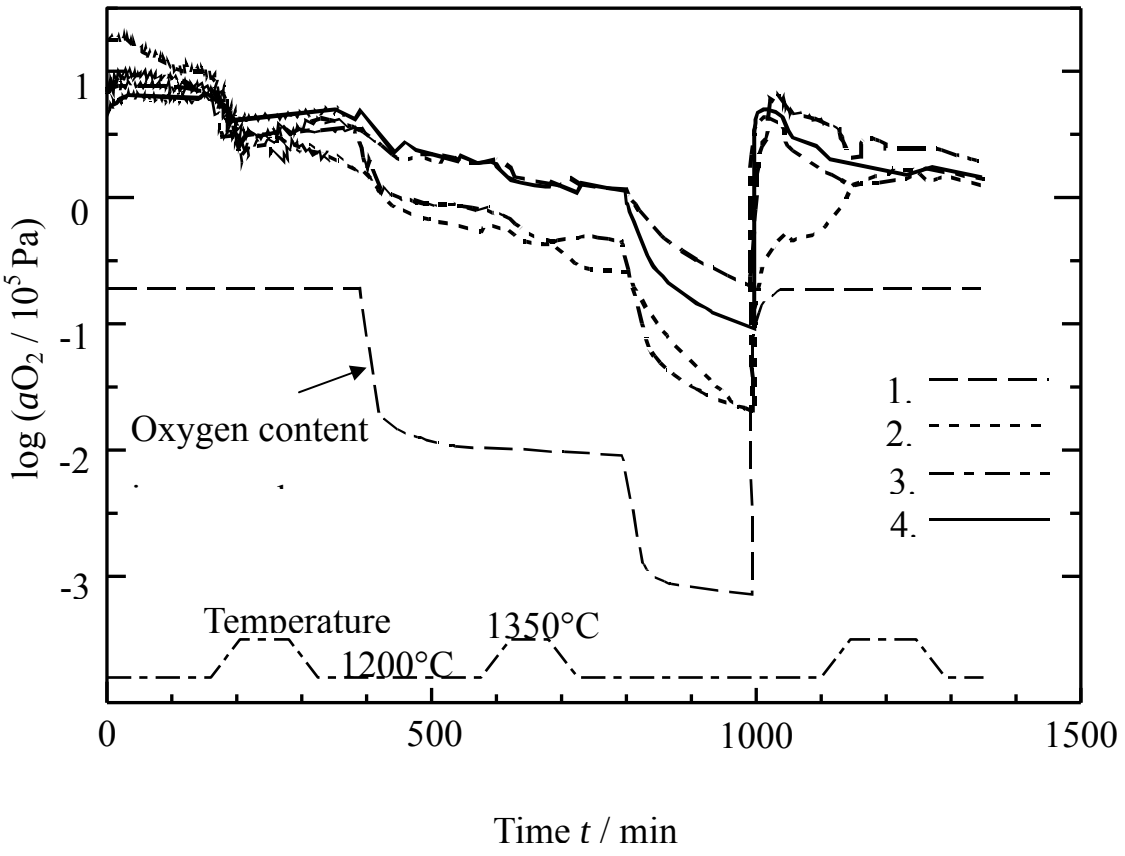

Fig. 4. Oxygen activity change in melt without additives. Four electrodes of type I in Fig. 3. were used. Atmosphere changed in order of air → N_2 with air → N_2 → air. Temperature change shown at bottom of figure.

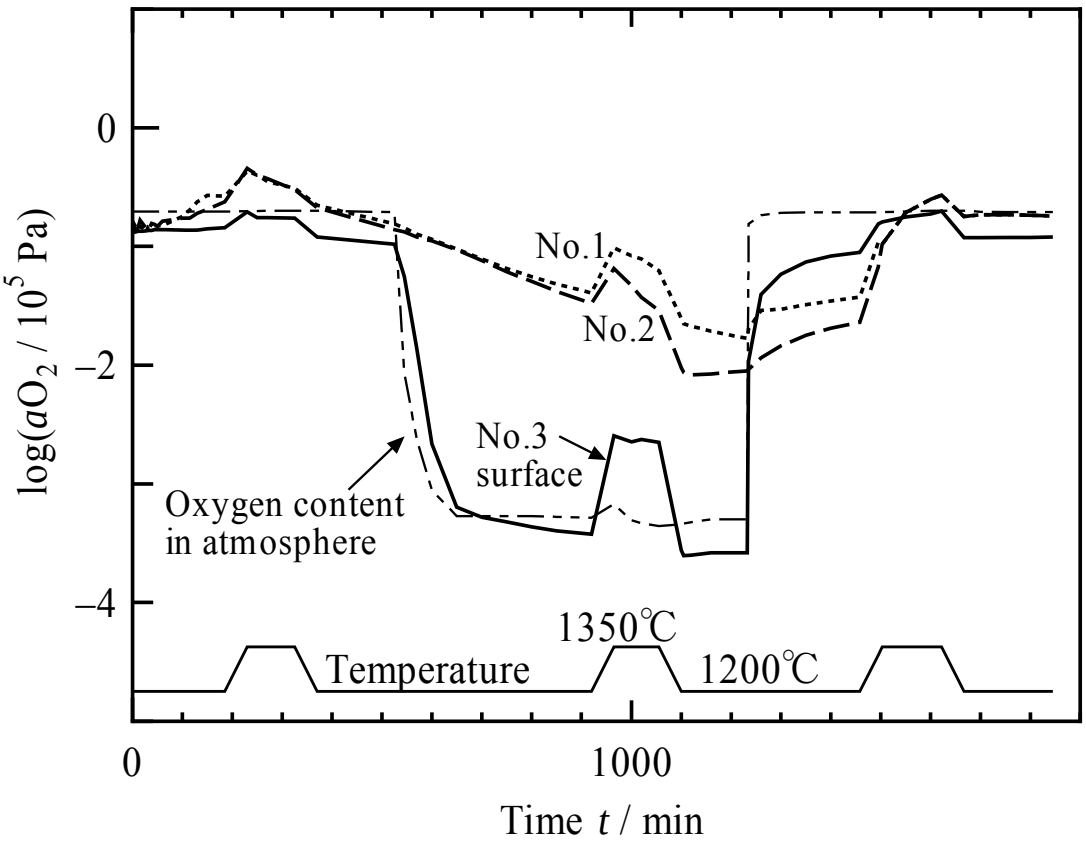

Fig. 5. Oxygen activity change in melt without additives. Two electrodes of type I (nos. 1 and 2) and one electrode of type II in Fig. 3 (no. 3) were used. Atmosphere changed in order of air → N_2 → air. Temperature change shown at bottom of figure.

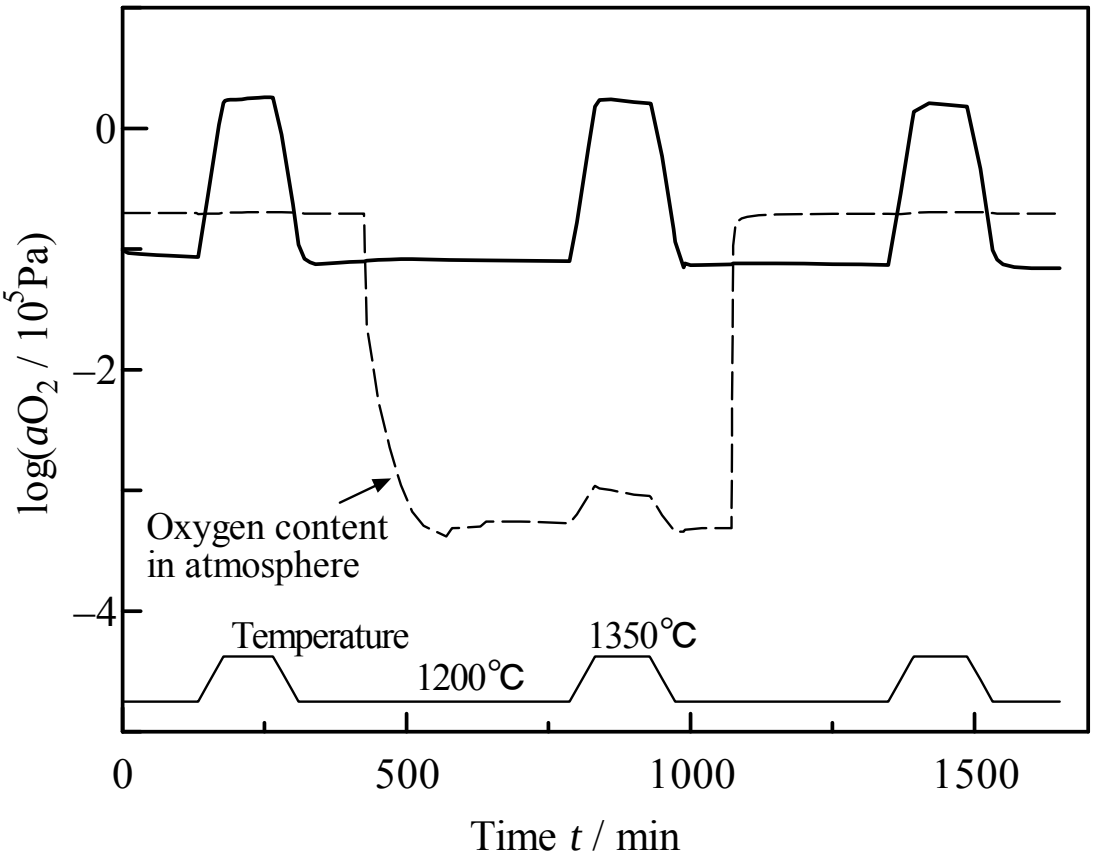

Fig. 6. Oxygen activity change in melt with 1 mol% Sb_2O_3. An electrode of type I was used. Atmosphere changed in order of air $\rightarrow$ N_2 $\rightarrow$ air. Temperature change shown at bottom of figure.

equilibrium (11), which moves to the right with increasing temperature. This behavior provides the basis for refining processes using redox elements such as antimony.[3,10] The results in the melts with 0.3 and 0.1 mol% of Sb_2O_3 are shown in Figs. 7 and 8, respectively. The initial activities were different in these figures. This may have been caused by a difference in the conditions of the batch melting or by carbon contamination in the casting process. The changing tendency of the oxygen activity in Figs. 7 and 8 was slightly different from the tendency in Fig. 6. The variation in the activity under changing temperature became larger as the antimony content increased. This is similar to the tendency of glass melt containing iron.[11] In contrast, the dependence of oxygen activity on oxygen content in the atmosphere became less significant with increasing antimony content. In the case of 1 mol% Sb_2O_3, even when the oxygen content in the atmosphere was changed from 0.2×10^5 Pa to 40 Pa, there was little change in oxygen activity in the bulk of the melt. This "buffering" phenomenon produced by Sb_2O_3 must be related to the reaction between oxygen and antimony as a redox element. When the oxygen activity dropped, the equilibrium (11) moved to the right, resulting in the production of Sb^{3+} and oxygen. This is the origin of the buffering effect.

The changes in oxygen activity in melt containing sulfate are shown in Figs. 9 and 10. When the temperature was raised, the activity increased and the value became unstable. This instability, which was reproducible in melt containing sulfate but not in other melts not containing sulfate, is probably due to bubbles of sulfur dioxide gas. The gas is produced by thermal decomposition of sulfate, which is written as

$$SO_4^{2-} \rightarrow SO_2 + 1/2\ O_2 + O^{2-} \qquad (12).$$

When the concentration of oxygen in the atmosphere was lowered, the activity of oxygen in the melt decreased slightly. This suggests that sulfate has a weaker buffer

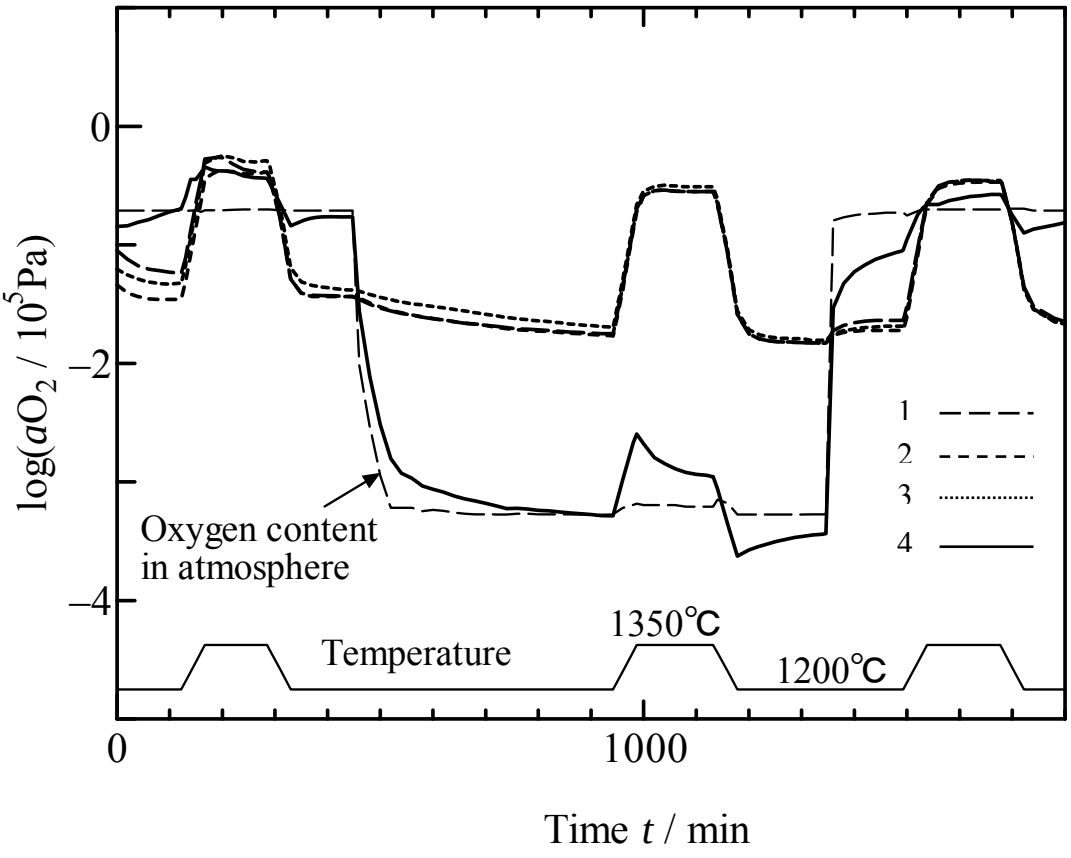

Fig. 7. Oxygen activity change in melt with 0.3 mol% Sb_2O_3. Three electrodes of type I (nos. 1 to 3) and one electrode of type II (no. 4) were used. Atmosphere changed in order of air $\rightarrow N_2 \rightarrow$ air. Temperature change shown at bottom of figure.

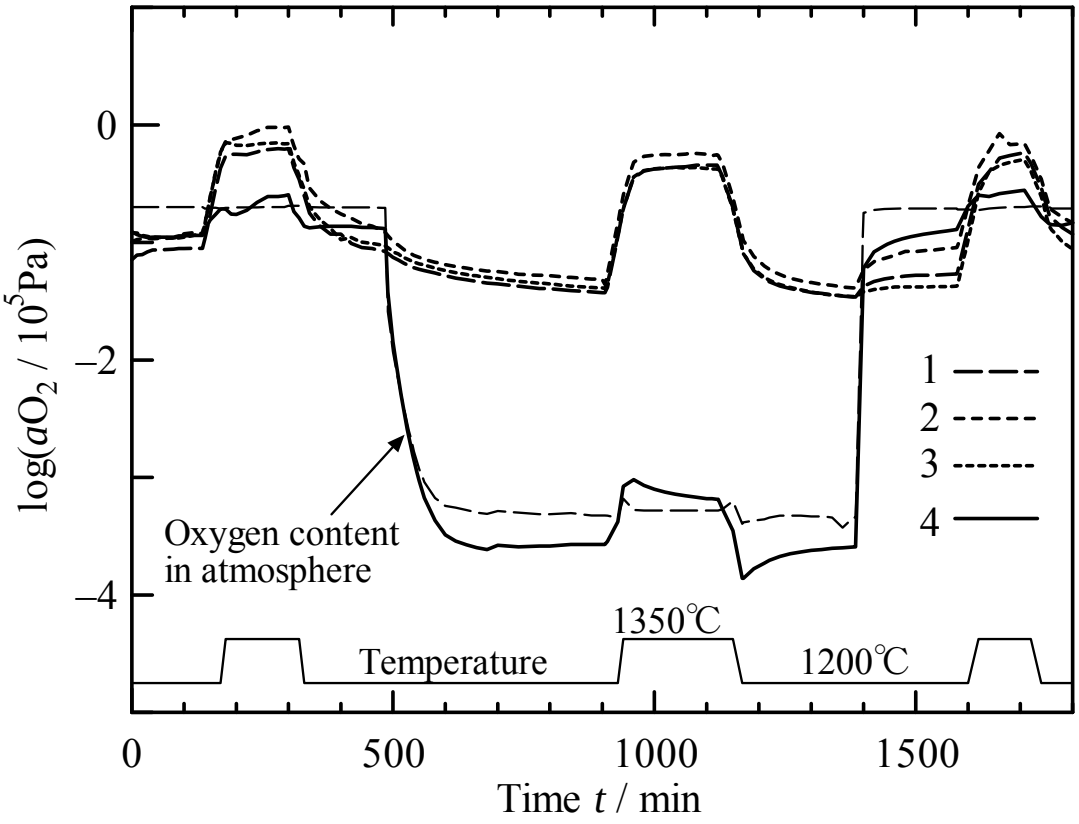

Fig. 8. Oxygen activity change in melt with 0.1 mol% Sb_2O_3. Three electrodes of type I (nos. 1 to 3), and one electrode of type II (no. 4), were used. Atmosphere changed in order of air $\rightarrow$ N_2 $\rightarrow$ air. Temperature change shown at bottom of figure.

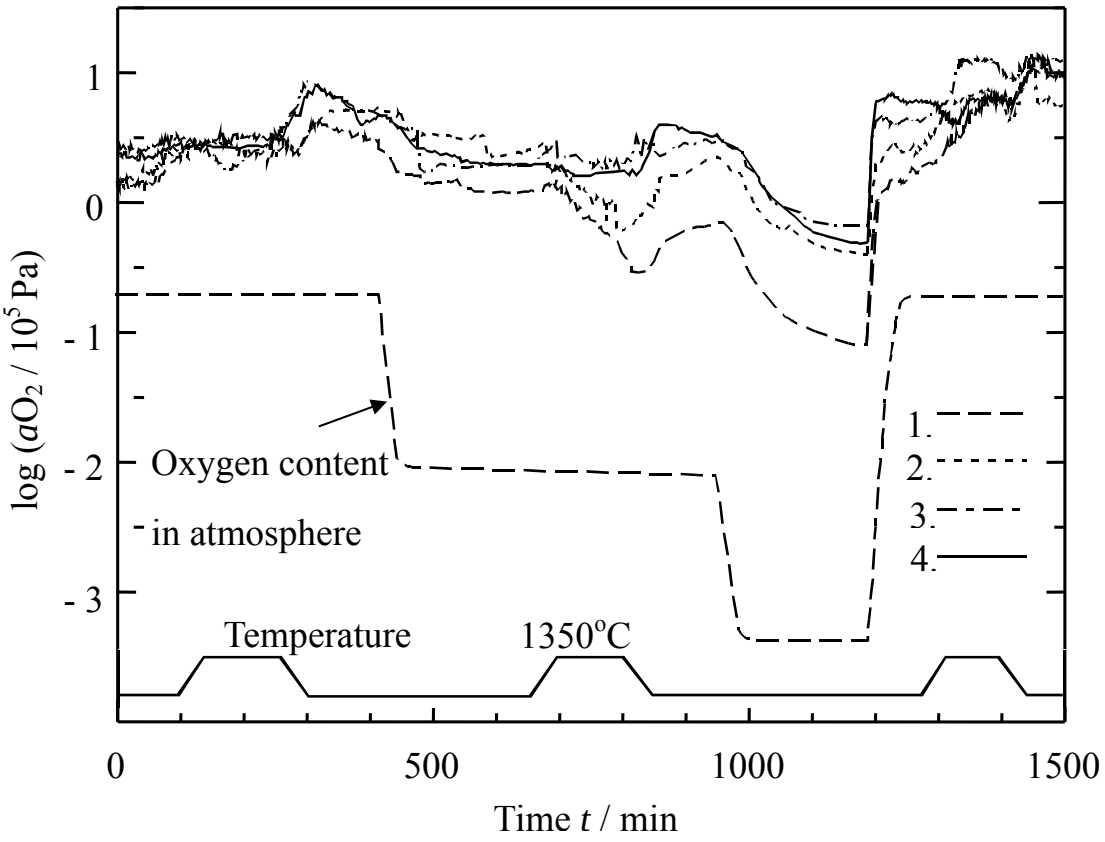

Fig. 9. Oxygen activity change in melt with sulfate. One mol% of sodium carbonate in the raw materials was replaced with sodium sulfate. Four electrodes of type I were used. Atmosphere changed in order of air → N_2 with air → N_2 → air. Temperature change shown at bottom of figure.

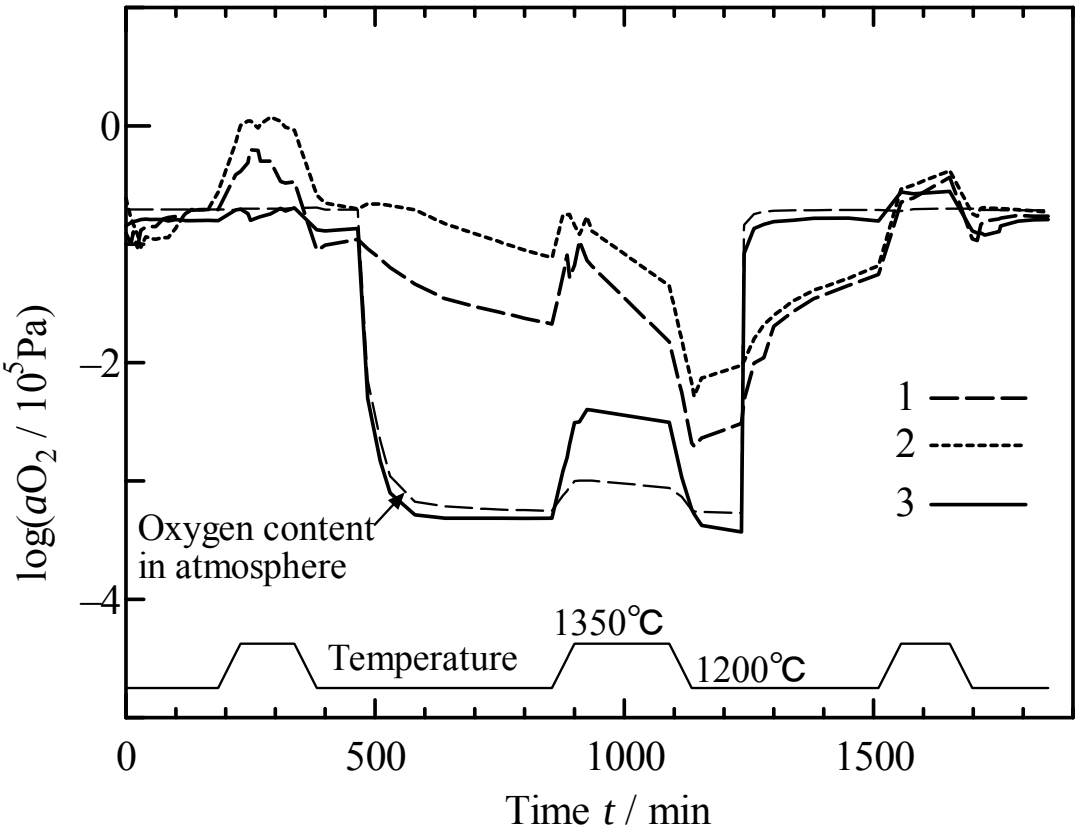

Fig. 10. Oxygen activity change in melt with sulfate. One mol% of sodium carbonate in raw materials was replaced with sodium sulfate. Two electrodes of type I and one of type II were used. Atmosphere changed in order of air → N_2 → air. Temperature change shown at bottom of figure.

effect than redox elements. As seen in Fig. 10, the oxygen activity decreased when the temperature was lowered. However, this kind of refining effect is not seen in melt containing sulfate[3] and was not observed in Fig. 9. Since the phenomenon has no reproducibility, the reason may again be the presence of redox contamination as in the melt with no additives.

2-5 Conclusion

Oxygen activity was measured using the EMF method in silicate glass melts with or without addition of refining agent. The effect of the refining agents was studied in detail under varying conditions of temperature and atmosphere. The results indicated that oxygen activity in the melt containing no refining agent changes with atmospheric variation but little with temperature variation. Oxygen activity in melt containing antimony changes with temperature variation and displays a buffer effect, but shows little change in response to atmospheric variation if the concentration of antimony is increased. Oxygen activity in melt containing sulfate as a refining agent changes with atmospheric variation and rises and becomes unstable with increasing temperature.

References

1. B. Stahlberg, B. D. Mosel, W. Müller-Warmuth and F. G. K. Baucke, *Glastech. Ber.*, **61**, 335-340 (1988).
2. J. Kappel, J. Bischof, F. Hutter and A. Kaiser, *Glastech. Ber.*, **64**, 109-114 (1991).
3. H. A. Schaeffer, T. Frey, I. Löh and F. G. K. Baucke, *J. Non-Cryst. Solids*, **49**, 179-188 (1982).
4. H. Müller-Simon and K. W. Mergler, *Glastech. Ber.*, **61**, 293 (1988).
5. M. Itoh, S. Sato and T. Yokokawa, *J. Chem. Thermodynamics*, **8**, 339 (1976).
6. J. G. Osteryoung and J. J. O'Dea, in: *Electroanalytical Chemistry*, ed. A. J. Bard, Vol. 14, Dekker, New York, (1986) p.209.
7. C. Rüssel and E. Freude, *Phys. Chem. Glasses*, **30**, 62-68 (1989).
8. T. Morita, H. Yamashita and T. Maekawa, *J. Ceram. Soc. Jpn.*, **102**, 419 (1994).
9. A. J. Bard and L. R. Faulkner, *Electrochemical Methods: Fundamentals and Applications*, Wiley, New York, (1980) p.160.
10. R. H. Doremus, *J. Am. Ceram. Soc.*, **43**, 655-661 (1960).
11. C. Rüssel, R. Kohl and H. A. Schaeffer, *Glastech. Ber.*, **61**, 209-213 (1988).

Chapter 3. Oxygen activity and redox state in glass melts.

3-1 Introduction

Iron is the most frequent impurity in commercial glass since it is commonly contained in low-purity raw materials. The effects of iron on the optical properties of glass have therefore been studied widely by many researchers.[1-7] Since iron has two redox states, Fe^{2+} and Fe^{3+}, with these states each having a different color, control of the redox condition during melting is important in adjusting the transmittance of glass in the wavelength regions of UV, visible light, and IR.[6,7] When glass melt is placed in a reductive environment, the content of Fe^{2+} increases and the glass turns bluish green because Fe^{2+} has a broad absorption band centered at 1100 nm. This absorption band is utilized in IR-cut glass such as cold filtered glass, which is produced under reductive conditions. When glass melt is placed in an oxidative environment, meanwhile, the iron in the glass is oxidized to the Fe^{3+} state and produces a yellowish color due to an absorption band which shows strong absorption below 380 nm that tails off towards longer wavelengths up to about 450 nm. Such glass containing Fe^{3+} in large amounts is used as UV-cut glass. The control of the redox states of Fe in glass is thus important for optical applications.

In order to control the redox states of iron in glass melt, other substances are usually added to the raw materials. Carbon or an organic reagent is used as a reducing agent, while nitrate or sulfate is added to glass as an oxidizing agent. Atmospheric control is also effective for the redox control of iron in glass. However, as the diffusion coefficient of oxygen in glass melt is less than 10^{-5} cm^2s^{-1},[8] atmospheric control is not effective after the formation of the melt unless the melt layer is very thin. It has been reported that, even in shallow melts, several hours are required to reach redox equilibrium by atmospheric control.[9] In contrast, atmospheric control is effective for powdery raw materials at temperatures below the melt formation.

For the above reasons, the heating modes used to make the melt from the raw material must affect the redox states of species in glass. To our knowledge, however, no relevant study has yet been carried out. Here, we report on the oxidation states of iron in glass and on the activity of oxygen in melts formed by two melting modes: gradual temperature increase and sudden temperature increase.

Oxygen activity in melts can be monitored by measuring electromotive force (EMF) using a Pt working electrode and a zirconia reference electrode.[10-12] A stabilized zirconia electrode is useful as the reference electrode for the measurement of oxygen activity because it transports oxide ions and its electric potential is determined by the oxygen concentration inside the electrode.[10-13] The zirconia electrode has been used to measure the redox potential of many ions in melts.[14,15]

Since the two redox elements have mutual interactions,[16] we also report on the effect of Sn addition on the redox states of iron in glass formed by the two melting modes.

3-2 Experimental Procedure

The composition of the base glass was $15.0Na_2O-11.3CaO-0.6Al_2O_3-73.1SiO_2$ (mol%). Reagent-grade powders of Na_2CO_3, $CaCO_3$, $Al(OH)_3$, and SiO_2 were used as the raw materials for glass containing Fe. Fe_2O_3 and SnO were used as additives. The raw materials were mixed thoroughly and melted in a high-purity alumina crucible (PSA-999) placed in an electric box furnace. We employed two heating modes. In Mode I, the temperature was raised at a rate of 5.6 ^oC/min from room temperature to 1400 ^oC. In Mode II, the raw materials were placed in a pre-heated crucible and immediately transferred to a furnace preheated to 1400^oC. In both modes, the melt in the crucible was observed from the top of the furnace through a viewing

port. The oxygen activity of the melt was measured using a Pt wire sealed in a silica tube and a stabilized zirconia electrode using air as the reference gas.[8] These electrodes were inserted into the raw materials when the powder surface started to melt. The voltage between the electrodes, ΔE, was monitored after they were immersed in the glass melt. The Pt electrode was set at a depth of about 10 mm from the melt surface. The oxygen activity, aO_2, was determined from the equation

$$aO_2 = 0.21 \exp(4F\Delta E/RT),$$

where F is the Faraday constant, R the gas constant, and T the absolute temperature. pO_2 in air gives 0.21 in the equation. Because of the slow diffusion of oxygen mentioned in the introduction above, the value of aO_2 differs in different parts of the melt if the melt is not perfectly homogeneous. A difference of more than 10 mV may be observed at different Pt electrode positions.

After measurement of the electromotive force for a certain period, the crucible was taken out of the furnace and kept at 560 ^{o}C for about 15 min, then cooled slowly to room temperature. A glass specimen was obtained by breaking the crucible. The obtained glass samples were sliced and polished to give two flat, parallel sides for the measurement of absorption spectra, which were obtained with a spectrophotometer (Model U-4100, Hitachi Co., Ltd. Tokyo).

In certain samples, the Fe content and the Fe^{2+}/total-Fe ratio were determined from wet analysis. The Fe^{2+} content was determined by means of redox titration of an HF solution in which the glass powder had been dissolved under an N_2 atmosphere, as described by Close *et al.*[17] For the analysis of total Fe amount, one gram of glass powder was dissolved in an HF-$HClO_4$ solution. After the powder had been completely dissolved in the mixed acid, the solution was evaporated and the residue dissolved in a certain volume of diluted HNO_3. The total Fe concentration in the solution was then

analyzed using an ICP (Model SPS7800, Seiko Instruments Inc. Chiba). It is estimated roughly that an error of a few percent may occur in the analysis.

To determine the redox state of Sn in glass samples, their Mössbauer spectra were measured using ^{119m}Sn as the gamma-ray source. The sample thickness was about 2 mm and the spectra were measured at room temperature with standard transmission geometry.

3-3 Results

3-3.1 *Redox state of Fe in glass*

Glass containing Fe is commonly greenish due to absorption of Fe^{2+} and Fe^{3+}. In samples containing both Fe and Sn, however, we found that the color depends strongly on the heating mode. Samples prepared from the raw materials by gradual heating to 1400 ^{o}C were green, whereas those prepared by rapid heating were blue. The UV-Vis-IR absorption spectra of these samples are shown in Fig. 1. Some discontinuity was seen at 850 cm^{-1} because the detector in the spectrophotometer was changed. This caused error of no more than 1 % in transmittance. Each spectrum was curve-fitted with several Gaussian and Lorentzian curves after the background level caused by reflection had been subtracted. The peaks at 3.26 eV, 2.98 eV, and 2.81 eV are attributed to Fe^{3+} and those below 2 eV to Fe^{2+}. Sample (a), which was prepared by heating gradually from room temperature, appeared to contain more Fe^{3+} than did Sample (b), which was prepared by rapid heating. The Fe^{2+}/total-Fe ratios of these samples, which were calculated from the ratio of the absorbance peak at 1.13 eV to that at 3.26 eV according to the method reported by Bamford,[2] were determined to be 10.9 % for Sample (a) and 74.2 % for Sample (b). This result indicates that the heating conditions strongly affect the redox states of Fe in glass.

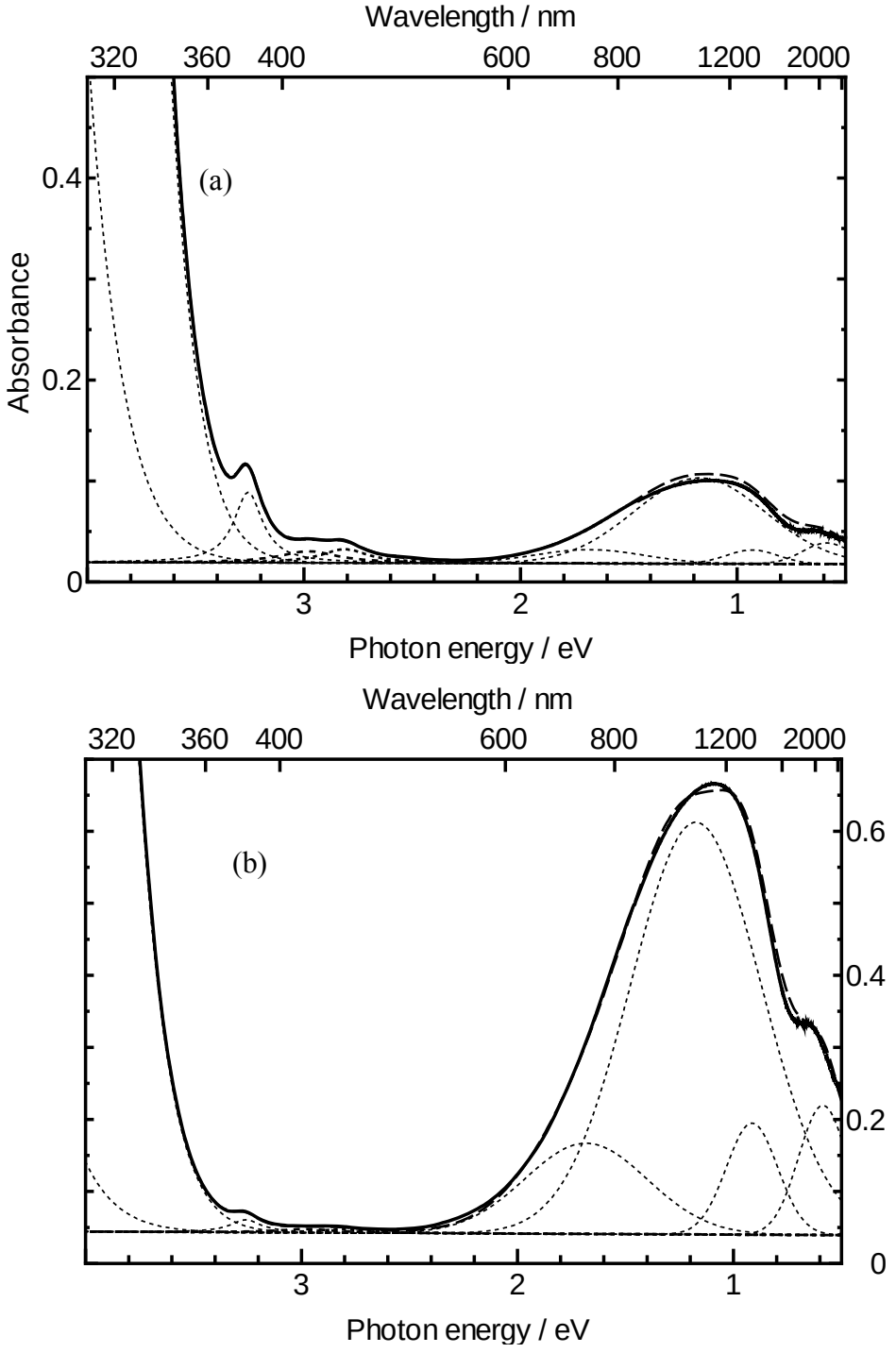

Fig. 1. Examples of UV-vis-IR spectra of glass samples containing Sn(0.76 mol%) and Fe (0.75 mol%) with Fe^{2+} to total Fe ratios of (a) 0.11 and (b) 0.74. The spectra are deconvoluted with Gaussian and Lorentzian lines. The absorbance is converted to the value for a sample thickness of 1 mm.

Table 1. Fe^{2+}/total-Fe ratios determined from absorption spectra and wet analysis for 3 glass samples. The samples contained 0.75 mol% Fe and no Sn. Samples (B) and (C) were prepared by remelting Fe-free cullet with addition of Fe_2O_3 and Fe_3O_4, respectively.

	Fe^{2+}/total Fe	
	Absorption spectrum	Wet analysis
(A)	0.094	0.103
(B)	0.175	0.183
(C)	0.386	0.396

In order to confirm the accuracy of the Fe^{2+} to total-Fe ratios determined from the absorption spectra, we compared them with those determined from wet analysis of the samples by the method described in the experimental section. In the comparison, we used glass samples containing different Fe^{2+} to total Fe ratios. The Fe^{2+}/total-Fe ratios determined from the absorption spectra and by wet analysis are summarized in Table 1. The results show that the Fe^{2+}/total-Fe ratios calculated from the spectra and those obtained from wet analysis agreed within the error limit of 1%. The estimation of the Fe^{2+}/total-Fe ratio based on absorption spectra is therefore concluded to be sufficiently accurate. Incidentally, the glass samples apparently containing a large amount of Fe^{2+}, Samples (B) and (C) in the table, were prepared by remelting the cullet in an N_2 atmosphere with addition of 0.75 mol% of iron in the form of Fe_2O_3 or Fe_3O_4.

Since we found that the Fe^{2+} to total Fe ratio determined from the absorption spectra was reliable, we used this method for the determination of the ratio in subsequent experiments, in which samples containing Fe and Sn at different concentrations were prepared using the two heating modes. The Fe^{2+} to total Fe ratios

Table 2. Fe^{2+}/total-Fe ratios in glass samples and oxygen activity in melts of samples prepared from raw materials containing different amounts of Fe as Fe_2O_3 and Sn as SnO. The samples were prepared by gradual heating (Mode I) or rapid heating (Mode II) (see caption of Fig. 3). The oxygen activity in the melts was monitored at 200 min after the temperature reached 1400 °C.

No.	Fe /mol%	Sn /mol%	Heating mode	Fe^{2+}/total Fe	log(aO_2)	Remarks
1	0.75	0	I	0.094	0.03	Table 1-(A)
2	0.75	0	II	0.117	-0.37	
3	0.04	0.45	I	0.235	-0.20	
4	0.04	0.45	II	0.628	-1.84	
5	0.75	0.76	I	0.109	0.12	Fig.1-(a)
6	0.75	0.76	II	0.742	-2.27	Fig.1-(b)

are shown in Table 2. The results show clearly that Samples 1, 3 and 5, which were heated gradually from room temperature, contain less Fe^{2+} than Samples 2, 4 and 6, which were heated rapidly to 1400 °C. The results also show that the addition of Sn leads to higher Fe^{2+} content in samples if prepared by heating rapidly. In contrast, this tendency is not clear in samples prepared by heating gradually, which show low Fe^{2+} to total Fe ratios irrespective of Fe content.

3-3.2 *Redox state of Sn in glass*

Mössbauer spectra were measured for the samples containing both Fe and Sn. The samples were prepared by gradual heating and rapid heating. For reference, we also measured the spectrum for P_2O_5-SnO glass in which most of the Sn ions were present as Sn^{2+}. The results showed that all the Sn ions in the samples containing both Fe and Sn were present as Sn^{4+} irrespective of the heating process, as shown in Fig. 2.

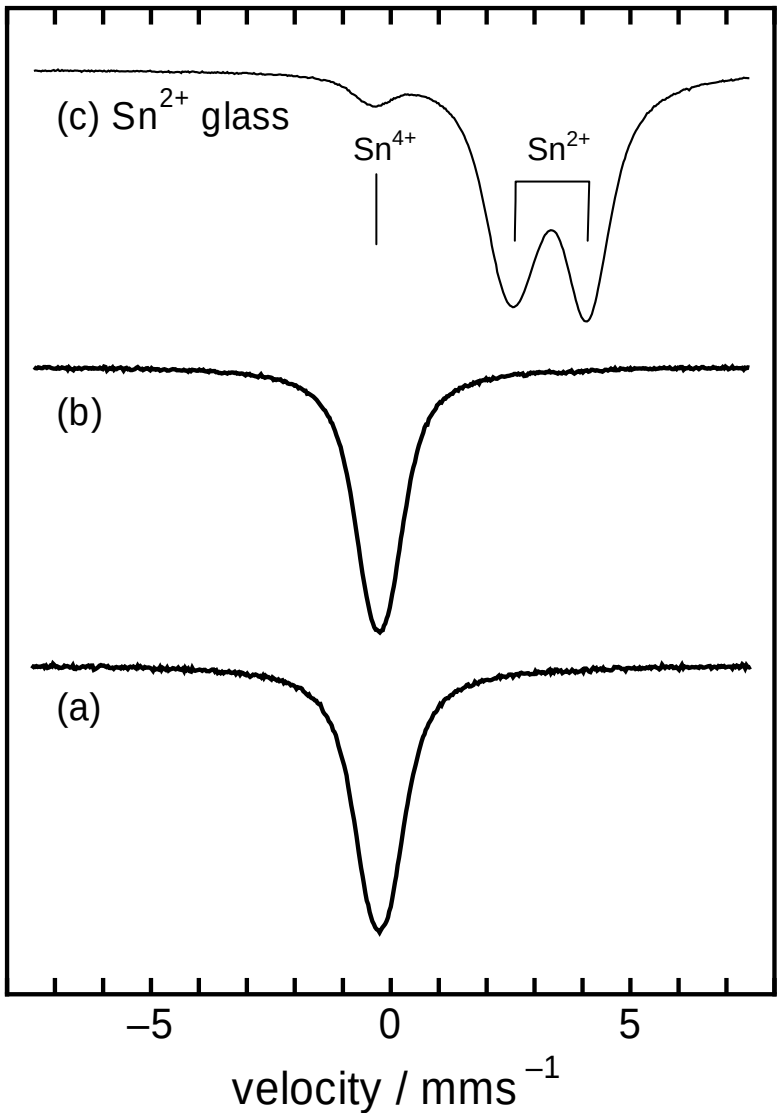

Fig. 2. Mössbauer spectra for glass samples containing Fe (0.75 mol%) and Sn (0.76 mol%), which were prepared by (a) Mode I (gradual heating), and (b) Mode II (rapid heating). Spectrum (c) is for a sample containing P_2O_5 and SnO in which most of the Sn was present as Sn^{2+}.

3-3.3 *Oxygen activity in melts*

The Fe^{2+} to total Fe ratio in the samples was expected to be affected by the concentration of oxygen in the samples during the heating process. We therefore measured the oxygen activity in the melts during the heating process using Pt and zirconia electrodes. Two heating modes were applied. In Mode I, the temperature was raised at a rate of 5.6 ^{o}C/min and the electrodes were immersed in the melt at approximately 1000 ^{o}C, at which the materials started to melt. In Mode II, the temperature was raised rapidly by placing the sample in a furnace preheated to 1400 ^{o}C, where they started to melt immediately, as observed through a viewing port.

The oxygen activity in the sample without the addition of Sn increased gradually with increase in temperature as shown by Line 1 in Fig. 3 in the time region before zero. When the temperature reached the plateau of 1400 ^{o}C, the oxygen activity leveled off after a slight overshoot. In contrast, when the sample was heated rapidly to 1400 ^{o}C, the oxygen activity in the melt was almost constant, as shown by Line 2, and was lower than the stationary value at 1400 ^{o}C for the sample heated gradually.

Figure 4 shows the oxygen activity of samples containing Fe as Fe_2O_3 and Sn as SnO. When the temperature of the sample was raised gradually, the oxygen activity rose with the increase in temperature and reached a constant value at 1400 ^{o}C, where the temperature was maintained, as shown by Lines 3 and 5. These two lines are for samples containing Fe and Sn at different concentrations. The oxygen activity profiles of these two samples were similar to each other and also to Line 1 in Fig. 3. The small difference in the oxygen activity between Lines 3 and 5 is attributable to a difference in the Sn/Fe ratios of these samples, which were about 11 and 1.0, respectively. When the temperature was raised rapidly, the oxygen activity was low, as shown by Lines 4 and 6. The values were generally much smaller than those of the samples not containing Sn

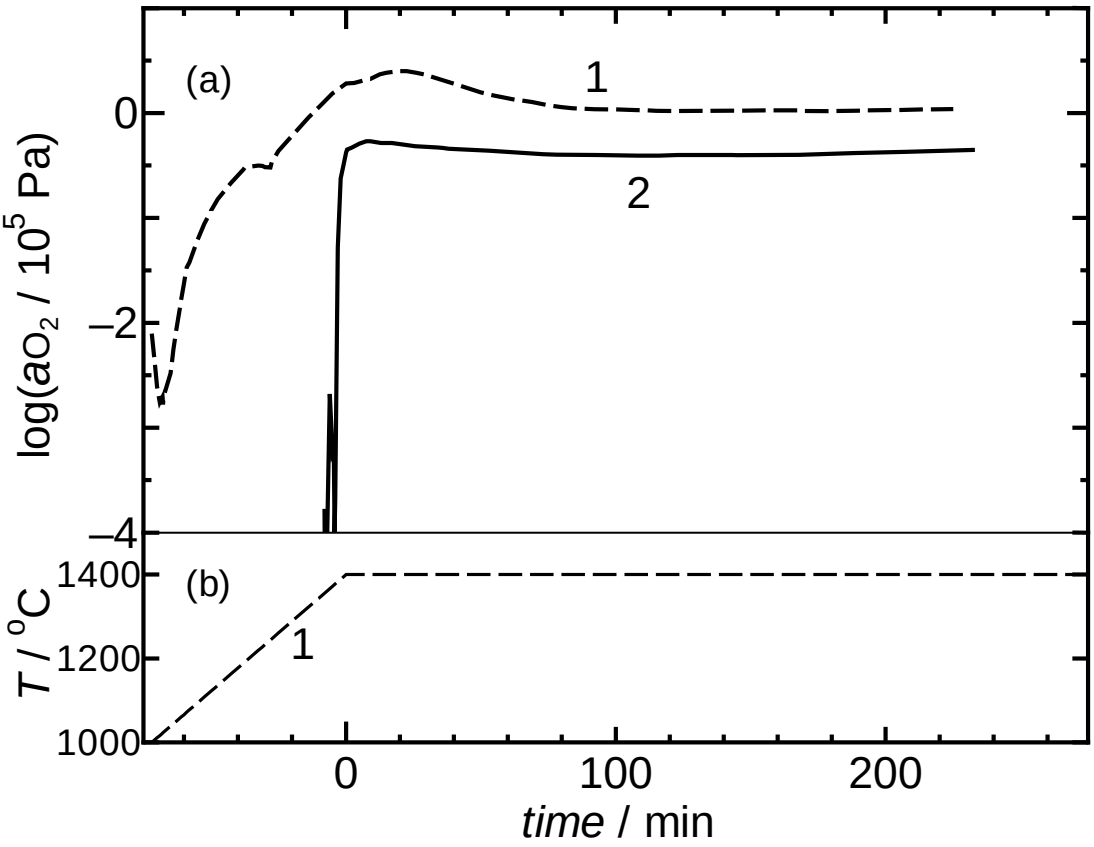

Fig. 3. (a) Change in oxygen activity in glass melts heated by two different modes and (b) temperature of melt. The raw material contained 0.75 mol% of Fe. The raw material was heated gradually at a rate of 5.6 ^{o}C/min to 1400 ^{o}C (Mode I) or rapidly in a furnace preheated to 1400 ^{o}C (Mode II). Lines 1 and 2 represent the data for the samples heated by Mode I and Mode II, respectively.

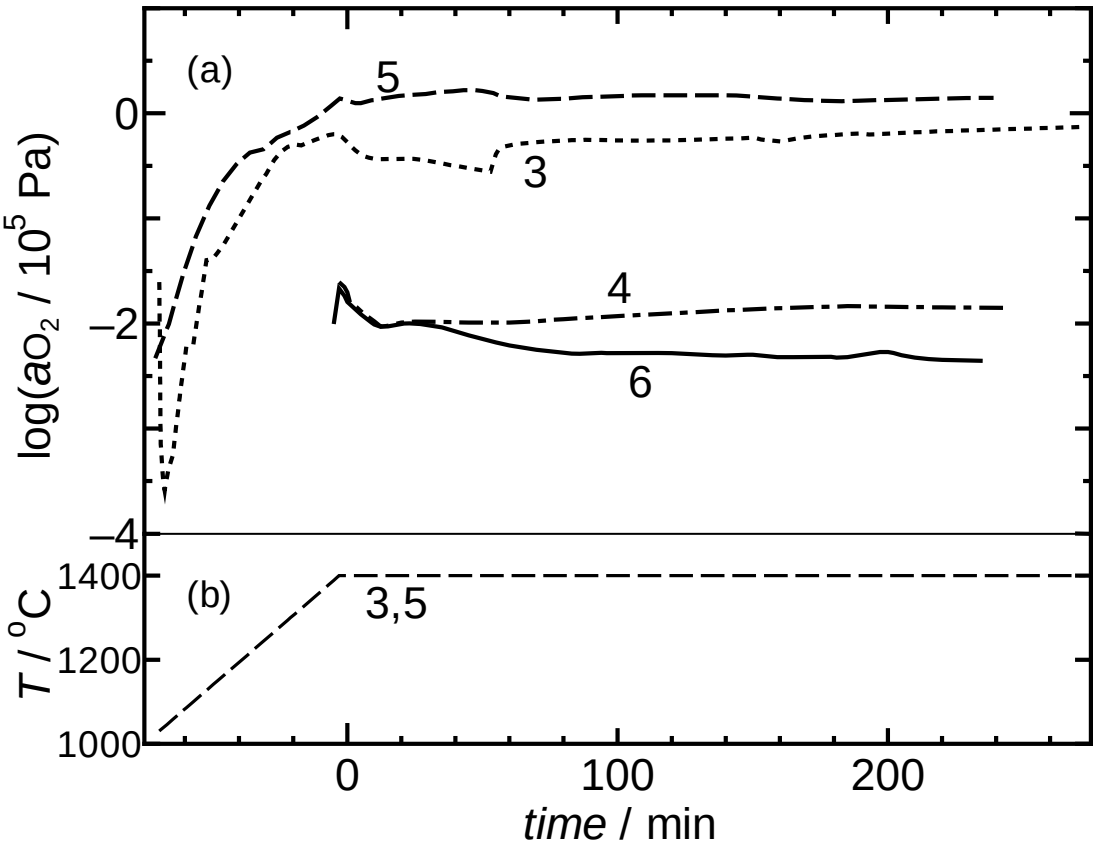

Fig. 4. (a) Change in oxygen activity in glass melts heated by two different modes and (b) temperature of melt. The raw materials contained 0.04 mol% Fe and 0.45 mol% Sn (Lines 3 and 4) or 0.75 mol% Fe and 0.76 mol% Sn (Lines 5 and 6). The raw materials were heated by Mode I (gradual heating) for Lines 3 and 5 and by Mode II (rapid heating) for Lines 4 and 6 (see caption of Fig. 3).

(see Line 2, Fig. 3). As will be discussed later, this is probably due to the reductive properties of the SnO added to the samples.

The ratio of Fe^{2+} to total Fe in glass samples prepared from raw materials containing different concentrations of Fe_2O_3 and SnO is shown in Table 2. For each set of concentrations, samples were prepared by gradual and by rapid heating. The oxygen activity of the melts is also shown in the table. A good correlation is observed between the Fe^{2+} to total Fe ratio and oxygen activity.

3-4 Discussion

The oxygen activity in melt containing Fe ions was expected to be determined by a number of factors: the atmosphere surrounding the melt, the redox species included in the material, and the equilibrium between oxygen and Fe ions. Oxygen activity may also be affected by the ease of oxygen molecule exchange with the atmosphere, which is affected by the conditions of the melt layer because the diffusion coefficient of oxygen in melt is very low.[8] If however the melt is agitated by bubbles formed in it, exchange will be accelerated.

Bubbles of CO_2 and H_2O are usually observed when the raw materials are heated and are due to the decomposition of materials such as Na_2CO_3. In the present study, when the samples were heated rapidly, bubbles were emitted vigorously from the melt for about 10 min. On the other hand, when the samples were heated gradually at the rate of 5.6 ^oC/min, the raw material partially melted at temperatures above 1000 ^oC and the bubbles appeared continuously at temperatures between 1050 and 1150 ^oC, at which a thick melt layer was formed. The bubbling stopped almost completely at temperatures higher than 1200 ^oC, at which the raw material melted completely. When the sample is heated gradually, the exchange between oxygen in the melt and that in the

atmosphere may thus be difficult at temperatures higher than 1150 ^{o}C.

At low temperatures before the formation of the melt, reaction between oxygen in the atmosphere and species in the raw material occurs easily, which affects the redox state of the species and the oxygen activity in the melt. The reaction between SnO particles and oxygen in the atmosphere was confirmed from the fact that, when the temperature was raised at the rate of 5 ^{o}C/min, the SnO powder was almost completely oxidized to SnO_2 in the furnace before the temperature reached 800 ^{o}C.

Oxygen is produced in the melt at elevated temperatures if the material contains Fe^{3+} as a result of a reaction with O^{2-}, which is abundantly present in the material. The equation is represented by

$$4Fe^{3+} + 2O^{2-} \rightleftarrows 4Fe^{2+} + O_2 \ . \qquad (1)$$

Since the equilibrium shifts to the right with the increase in temperature,[18] the oxygen activity in the melt will increase with temperature, as observed when the temperature was raised gradually (see Line 1, Fig. 3 and Lines 3 and 5, Fig. 4). Such phenomena are well known in melts containing redox species.[10] If the amount of oxygen included in the melt is small, the reaction of Equation (1), even if it is very small, will cause a large change in the oxygen activity.

After the formation of the melt layer on the raw materials, the release of oxygen from the material to the atmosphere is prevented due to the low diffusion coefficient of oxygen in the melt. This is especially important when the sample is heated gradually and when temperatures have reached 1150 ^{o}C. Under such conditions, because of the high oxygen activity, the reaction represented by equilibrium (1) is suppressed and the concentration of Fe^{2+} in the melt is kept low. On the other hand, when the sample is heated rapidly to 1400 ^{o}C, the reaction in Equation (1) occurs at the same time as the emission of CO_2 and H_2O. The melt layer formed on the surface of the

samples is therefore agitated and stirred by gas emission, which can be observed visually. This allows the release of oxygen from the sample to the atmosphere and promotes the reaction in Equation (1), leading to a lower oxygen activity in the melt and higher concentration of Fe^{2+} in the glass. These tendencies are consistent with the experimental results (see entry numbers 1 and 2 in Table 1).

When the sample contains SnO together with Fe as Fe_2O_3, the reaction between Sn^{2+} and Fe^{3+} will affect the content of Fe^{3+} in the glass. However, Sn^{2+} also reacts with oxygen, which is expressed by

$$SnO + 1/2O_2 \rightleftarrows SnO_2 \quad . \qquad (2)$$

The forward process of Equation (2) is likely to occur at relatively low temperatures below 1000 ^oC, as described before. Thus, if the materials are heated gradually, the SnO in the materials is converted to SnO_2 before the melting is complete and has little influence on the concentration of Fe^{3+} in the glass. In contrast, when the materials are heated rapidly, Sn^{2+} remains in the melt in which the reaction in Equation (1) takes place. Under such conditions, the Sn^{2+} and Fe^{3+} in the melt react, leading to an increase in Fe^{2+} and decrease in Fe^{3+}. This reaction is represented by

$$2Fe^{3+} + Sn^{2+} \rightleftarrows 2Fe^{2+} + Sn^{4+}. \qquad (3)$$

This reaction must have proceeded all the way to the right during cooling since no Sn^{2+} was detected in the glasses after cooling by Mössbauer analysis. All the above propositions based on the reactions in Equations (1) – (3) are consistent with the Fe^{2+} to total Fe ratios shown in Table 2. We will now discuss the oxygen activity in the melt. The oxygen activities and Fe^{2+} to total Fe ratios, which are presented in Table 2, show good correlation. This suggests that the equilibrium expressed by Equation (1) controls the concentrations of oxygen, Fe^{2+}, and Fe^{3+} in the melts and that the Fe^{2+} to total Fe ratio is maintained in the glass produced. When the melt is annealed and cooled down

after heating to 1400 °C, the reverse reaction of Equation (1) may occur. However, the results suggest that the total amount of oxygen diffused into the melt from the atmosphere is not large enough to affect the Fe^{2+} to total Fe ratio except in samples containing only a small amount of Fe_2O_3 (entry number 3 in Table 2).

3-5 Conclusion

Soda-lime silicate glass samples containing iron were melted by gradual heating to 1400 °C or rapid heating at 1400 °C and the difference in oxygen activity measured. The redox state of iron in the glass was measured by optical absorption spectroscopy. When the raw materials were heated gradually at a rate of 5.6 °C/min, oxygen activities were approximately 1×10^5 Pa, which indicates that the melt was saturated with oxygen. This is because oxygen released from the raw material at high temperatures remained in the melt due to its low oxygen diffusion coefficient. When the raw material was heated rapidly at 1400 °C, the oxygen activity in the melt was lowered to about 0.4×10^5 Pa because the melt was vigorously agitated by bubbles of CO_2 and H_2O. When SnO was added to the raw material, the oxidation state of Fe was strongly affected by the heating mode: the Fe^{2+} to total Fe ratio exceeded 60% following rapid heating, but was lower than 25% after gradual heating. The oxygen activity in the melt was also strongly affected by the heating mode. When heated gradually, a large part of the SnO in the raw material was oxidized by atmospheric oxygen before the formation of the melt. This led to a weakened reductive environment in the melt and high Fe^{3+} content in the glass. On the other hand, when heated rapidly, a large amount of the Sn^{2+} remained in the melt and reduced Fe^{3+} to Fe^{2+}. These findings are important because the heating speed of raw materials strongly affects the oxidation state of Fe contained in glass and therefore its optical properties.

References

1. W. A. Weyl, *Coloured Glasses*, Dawson's of Pall Mall, London, 1959.
2. C. R. Bamford, "Ionic Colouration by Transition Metals and Ligand Field Theory"; pp. 33-66 in *Glass Science and Technology*, Vol. 2, *Colour Generation and Control in Glass*. Elsevier Scientific Publishing Company, Amsterdam, 1977.
3. F. N. Steele and R. W. Douglas, *Phys. Chem. Glasses*, 6 (1965) 246-252.
4. P. A. Bingham, J. M. Parker, T. Searle, J. M. Williams and K. Fyles, *J. Non-Cryst. Solids*, 253 (1999) 203-209.
5. J. E. Fenstermacher, *J. Non-Cryst. Solids*, 38&39 (1980) 239-244.
6. K. M. Fyles, *Glass Technol*., 37 (1996) 2-6.
7. T. Uchino, K. Nakaguchi, Y. Nagashima and T. Kondo, *J. Non-Cryst. Solids*, 261 (2000) 72-78.
8. M. Yamashita, *Phys. Chem. Glasses*, 45 (2004) 355-360.
9. M. Iwase, T. Okumura, K. Kawamura, Y. Miyamoto and H. Oh-uchi, *Glass Technol*., 39 (1998) 142-146.
10. T. Tran and M. P. Brungs, *Phys. Chem. Glasses*, 21 (1980) 178-183.
11. H. A. Schaeffer, T. Frey, I. Löh and F. G. K. Baucke, *J. Non-Cryst. Solids*, 49 (1982) 179-188.
12. V. A. Lenhart and H. A. Schaeffer, *Glastech. Ber*., 58 (1985) 139-147.
13. M. Sasabe and K. Goto, *Metall. Trans*., 5 (1974) 2225-2233.
14. C. Montel, C. Rüssel and E. Freude, *Glastech. Ber*., 61 (1988) 59-63.
15. C. Rüssel and G. von der Gönna, *J. Non-Cryst. Solids*, 260 (1999) 147-154.
16. H. D. Schreiber, L. J. Peters, J. W. Beckman and C. W. Schreiber, *Glastech. Ber. Glass Sci. Technol.*, 69 (1996) 269-277.

17. P. Close, H. M. Shepherd and C. H. Drummond, *J. Am. Ceram. Soc*., 41 (1958) 455-460.

18. A. Paul, *Chemistry of Glass*, London, New York, Chapman and Hall 1982. p. 226.

Chapter 4. Oxygen diffusion in glass melts.

4-1 Introduction

The mechanism of bubble formation and disappearance in glass melt is an essential subject to be clarified for the understanding of glass refining process. Many studies have been carried out for bubble formation,[1] gas solubility in melts,[2-4] bubble shrinkage[5] etc. In the refining process, a refining agent such as arsenic oxide or sodium sulfate plays an important role for bubble reduction. During the process, the agent produces oxygen, which expands bubbles and eases them to move toward the melt surface.[6] Bubble shrinkage and expansion have been treated in many studies[7-10] and equations for diffusion and reaction have been proposed.[11-15] If there were an accurate value for the oxygen diffusion coefficient in the melt, these evaluations would be more precise. However, there have not been many attempts to measure the diffusion coefficient since the high temperature makes it difficult to measure many properties. Moreover, since most of the oxygen contained in melts exists as oxide ions, it is difficult to distinguish the molecularly dissolved oxygen from the ions. Probably for this reason, diffusion coefficients measured using a tracer by means of mass analysis[16] or proton activation analysis[17] were much smaller than that measured by bubble shrinkage[7]; the former methods measured the total oxygen diffusion, while the latter focused on oxygen molecules.

During the past two decades, oxygen activity in melts has been measured by the electromotive force (EMF) method with zirconia and platinum electrodes.[18-20] The refining process for arsenic oxide-containing melts could be easily understood from the result by this method: Raising the temperature increases the oxygen activity in the melt, which expands the bubbles, causing them to rise to the surface. Falling temperature lowers the activity, which reduces the residual bubbles. Other redox elements such as antimony oxide and transition metal ions have a similar effect though the effective

temperature is different and the effectiveness is low in ordinary silicate melts.

Using the EMF method, the diffusion of oxygen can be measured:[21,22] When the oxygen content in the atmosphere is changed, the oxygen activity in the melt changes by diffusion and the EMF changes. In these studies, the obtained diffusion coefficients were very large compared with other results. The oxygen concentration change using this method can be written as[23]

$$\frac{C}{C_0} = \frac{4}{\pi} \cdot \sum_{n=0}^{\infty} \frac{(-1)^n}{2n+1} \exp\left[\frac{-D(2n+1)^2 \pi^2 t}{4h^2} \right] \qquad (1),$$

when the electrode is located on the bottom. In this equation, C is the oxygen concentration, C_0 the initial concentration, D the diffusion coefficient, h the melt depth and t the time after atmosphere change. By comparing equation (1) and a simplified equation at t >> 0,[22] an incubation time t_I can be determined. This is the period needed for transmission of detectable concentration change by diffusion; after this period the EMF will start to change. In cases where the incubation time was not observed,[22] some error might be included in the experimental procedure.

Equation (1) is valid if no polyvalent element is contained in the melt. Since polyvalent elements react with oxygen, they exert a buffer effect on the oxygen activity. When oxygen activity decreases with diffusion, the element will turn to a lower valence state and an oxygen molecule will be produced. This effect suppresses the voltage change in the EMF method and leads to a lower apparent diffusion coefficient.[24] In the case of bubble shrinkage measurement, oxygen physically dissolved near the bubble reacts with the element of the lower valence state, leading to a higher apparent diffusion coefficient. Hence, for oxygen diffusion in the case of a melt containing a polyvalent element, this reaction and the diffusion of the polyvalent element, which is considered

to be a part of the chemically dissolved oxygen, should be taken into account.

The diffusion of polyvalent elements has been measured with voltammetric techniques such as cyclic voltammetry[25] and square wave voltammetry.[26-28] Results of these studies show that the diffusion coefficients of polyvalent elements were one to two orders of magnitude lower than those of alkalis. The redox potentials of these elements were also measured by the same method. These values are important for the redox conditions of these elements and for the refining process.

The solubility of oxygen in a melt is also important. If the value of physically dissolved oxygen is much lower than the concentration of a polyvalent element, the buffer effect mentioned above becomes predominant compared with the oxygen diffusion. If the diffusion coefficient of oxygen molecules is the same in melts with and without polyvalent elements, it will be valuable to measure the coefficient in the melt without the element since it would be difficult to measure the value in the melt with the element.

In this study, the experimental method for EMF measurement is investigated. The oxygen diffusion coefficient was estimated by comparing the experimental and calculated results. The reaction of antimony as a polyvalent element was also examined. The procedure, results and remaining experimental problems are discussed below.

4-2 Experimental

The glass composition was $20Na_2O$-$10CaO$-$70SiO_2$. Reagent grade Na_2CO_3, $CaCO_3$ and SiO_2 were weighed and mixed thoroughly in a mortar and melted in a Pt crucible at 1400 ^oC in an electric furnace, then cast in a graphite mold. The glass blocks were placed in a cylindrical alumina crucible (SSA-S, Nikkato) 40 mm in diameter.

After setting a Pt and a zirconia electrode, the glass was remelted inside a vertical alumina tube 70 mm in diameter in an electric furnace. Antimony-containing glass was prepared by adding 1 mol % of Sb_2O_3 to the described mixture.

Figure 1 shows the structure of the Pt electrode. A Pt wire 1.5 mm in diameter with a Pt plate was heated and vacuum-sealed in a silica tube 5 mm in outer-diameter and 2 mm in inner-diameter. The silica tube was required as an insulator to avoid an

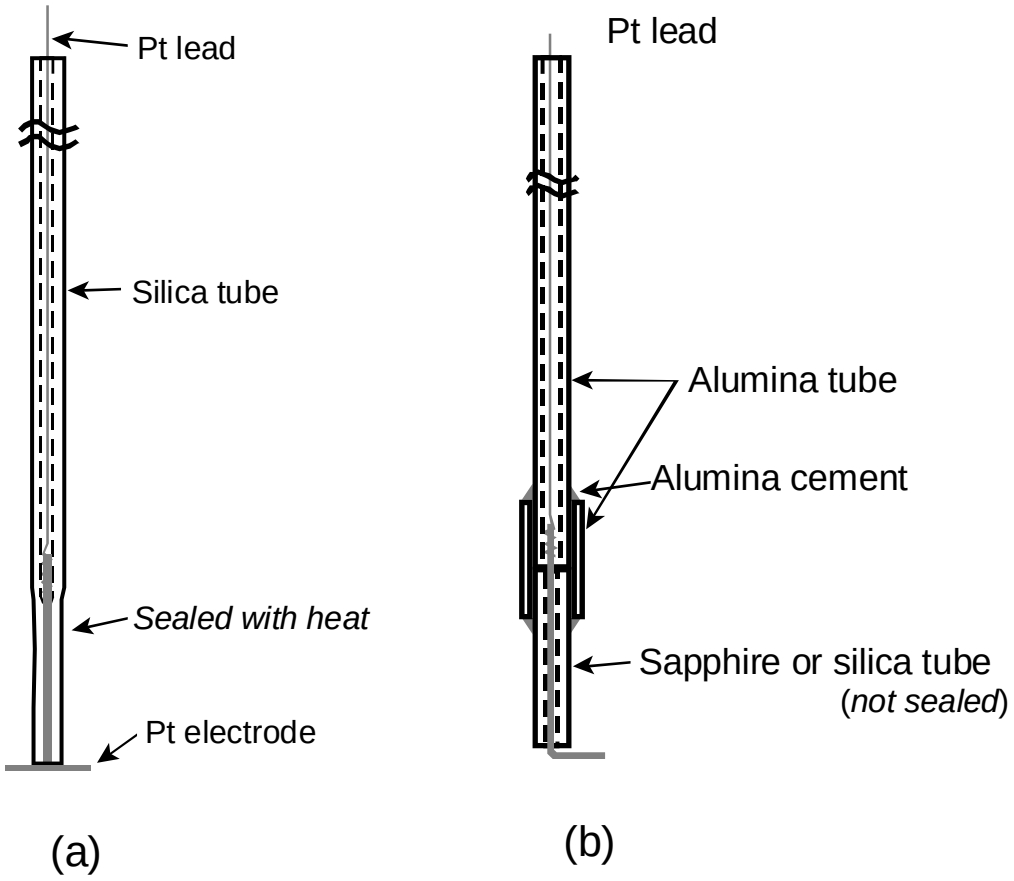

Fig. 1. Structures of Pt electrodes for (a) oxygen diffusion measurements and (b) comparing materials used as insulators.

oxygen redox reaction on the Pt lead at the melt-air interface. For comparison of insulating materials, a silica tube or sapphire (alumina single crystal) tube having a hole of 1.5 mm ϕ (Kyocera) was used and connected to an alumina tube (SSA-S, Nikkato) with alumina cement (Aron ceramic D, Toagosei) as shown in Fig. 1-b. A Pt wire 1.5 mm in diameter was used as an electrode in this case. The structures of the zirconia electrode and O_2 sensor made of zirconia have been described in chapter 2. Dry air (mixture of 20% O_2 and 80% N_2) was passed over these zirconia electrodes as a reference gas.

The furnace had a slight temperature gradient of 0.4°C/cm, with the upper level at a higher temperature to avoid convection. Dry air (mixture of 20% O_2 and 80% N_2) or N_2 gas was passed through the tube at a rate of 500 cm^3/min. For accurate measurement of the diffusion coefficient, the Pt electrode position had to be precisely determined. For this purpose, a Pt wire was immersed at the edge of the crucible and the electrodes were slowly dropped with a screw while measuring AC impedance with an LCR meter (hp 4262, Hewlett-Packard) between the electrodes and the Pt wire. The surface position of the melt was detected by a sudden drop of impedance. The Pt electrode was dropped at a preset position and the zirconia electrode was set at the surface of the melt. EMF (ΔE) was measured between the platinum electrode and a platinum wire connected to the zirconia electrode with a digital voltmeter (2114H, Advantest). The schematic electrode configuration is shown in Fig. 2. After raising the temperature, air was passed for at least 20 h to stabilize the EMF value, and the atmosphere was changed to N_2 for several hours, then changed to air again.

Oxygen activity in the melt (aO_2) was calculated from the equation

$$\Delta E = (RT/4F) \ln(aO_2 / pO_2) \qquad (2)$$

where R is the gas constant, T the absolute temperature, F the Faraday constant and the

pO_2 of the zirconia electrode is set at 0.2.

4-3 Calculation

First, oxygen diffusion without polyvalent elements was considered. Oxygen diffusion in the melt was assumed to be one dimensional from the surface. Let x be the vertical direction, $x = 0$ the surface position, $x = L$ the depth of melt and $x = x_e$ the position of the electrode. The melt is divided into small increments Δx, and $[O_2]|_N$ is the oxygen concentration at a distance $N\Delta x$ from the surface of the melt. Assuming a constant diffusion coefficient of oxygen, D, the oxygen concentration change is calculated numerically with Fick's equation,

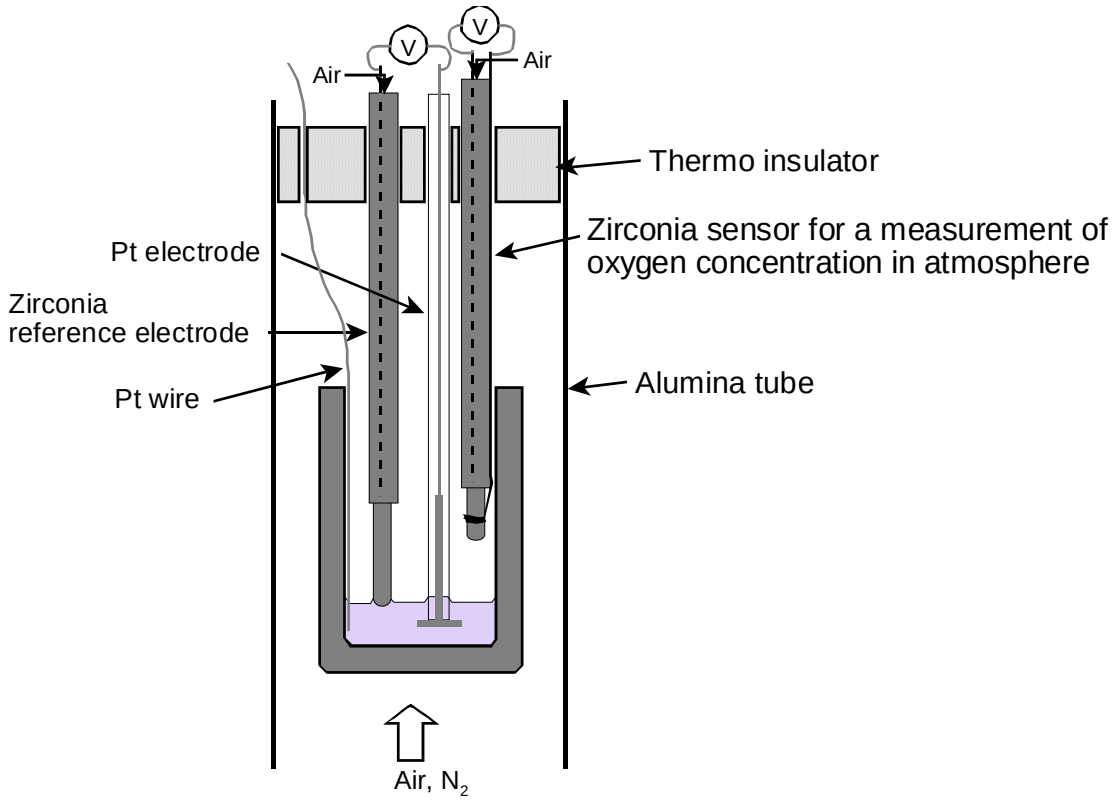

Fig. 2. Schematic cell configuration.

$$\Delta[O_2]|_N = \Delta t\left(D\frac{[O_2]|_{N-1} - 2[O_2]|_N + [O_2]|_{N+1}}{\Delta x^2} \right) \quad (3)$$

The oxygen concentration, $[O_2]$, is considered to be proportional to the oxygen activity, aO_2, as shown in the equation,

$$aO_2 = [O_2] / [O_2]_{satd.} \quad (4),$$

where $[O_2]_{satd.}$ is the saturated concentration of physically dissolved oxygen in a melt at a temperature when the partial pressure of oxygen is unity. Though the $[O_2]_{satd.}$ value is decided by the Henry's law, it is not necessary to consider the value since it is canceled in equation (3). As initial and boundary conditions,

$$aO_2 = 0.2 \qquad (t = 0,\ 0 < x < L) \quad (5)$$

$$\partial[O_2] / \partial x = 0 \qquad (x = L) \quad (6).$$

At the melt surface, oxygen activity was assumed to be the same as in the atmosphere. Hence, the oxygen activity at the surface, $aO_2|_s$, is equilibrated to the atmosphere, as

$$aO_2|_s = pO_2 \text{ in atmosphere} \quad (7).$$

The calculation was repeated from $x = 0$ to $x = L$ and from $t = 0$ to some period for several D values, and the oxygen concentration changes at $x = x_e$ were recorded. ΔE values were obtained from equation (2). A smaller Δx or Δt was confirmed not to change the resultant curve.

If antimony is contained in the melt as a polyvalent element, it reacts to oxygen with the following equation:

$$Sb^{3+} + 1/2O_2 \rightleftarrows Sb^{5+} + O^{2-} \quad (8).$$

The change of oxygen concentration at any point in the melt is expressed with the equation

$$\Delta[O_2] = \Delta[O_2]_{diff} + \Delta[O_2]_{react} \quad (9),$$

which can be treated as a case of diffusion with reaction.[23] The diffusion term indicates

a movement of physically dissolved oxygen and the reaction term represents the contribution of chemically dissolved oxygen. If the diffusion of antimony is ignored,

$$\Delta[O_2]_{react} = 1/2\ \Delta[Sb^{3+}] = -1/2\ \Delta[Sb^{5+}] \quad (10).$$

Since the diffusion coefficient of antimony was around 10^{-8} cm^2s^{-1} at 1200°C,[26-28] this assumption will be valid if the oxygen diffusion coefficient is larger than 1×10^{-7} cm^2s^{-1} at this temperature. The change in oxygen concentration becomes

$$\partial[O_2] / \partial t = D\ \partial^2[O_2] / \partial x^2 - 1/2\ \partial[Sb^{5+}] / \partial t \quad (11).^{24}$$

When reaction rates, k_f for the right hand and k_b for the left hand in equation (8), are introduced and $[O^{2-}]$ is considered to be constant, the concentration change of antimony becomes

$$\partial[Sb^{5+}] / \partial t = k_f\,[Sb^{3+}][O_2]^{1/2} - k_b\,[Sb^{5+}] \quad (12).$$

Here, $[Sb^{3+}]$ becomes $[Sb_{total}] - [Sb^{5+}]$. From equations (11) and (12), the oxygen concentration change can be numerically calculated using an equation similar to equation (3). The D value, $[O_2]_{satd.}$, $[Sb^{5+}]/[Sb^{3+}]$ at $t = 0$, k_f and k_f / k_b should be considered to simulate the oxygen concentration change in this case.

4-4 Results and Discussion

Figure 3 shows the results of our comparison of insulating materials. The x axis shows time and y axis shows the observed EMF values and calculated ΔE values. Since a complete sealing between sapphire and Pt was impossible, the silica tube was not sealed so that conditions would be uniform. Electrodes were set 4 mm from the melt surface. The dot-dashed line is the oxygen content in the atmosphere, which was changed from dry air to N_2 and from N_2 to air. When N_2 was introduced above the glass melt, the EMF value on the electrode with sapphire started to drop within 1 min as shown in curve b, while the value on the electrode with silica, shown in curve a, showed

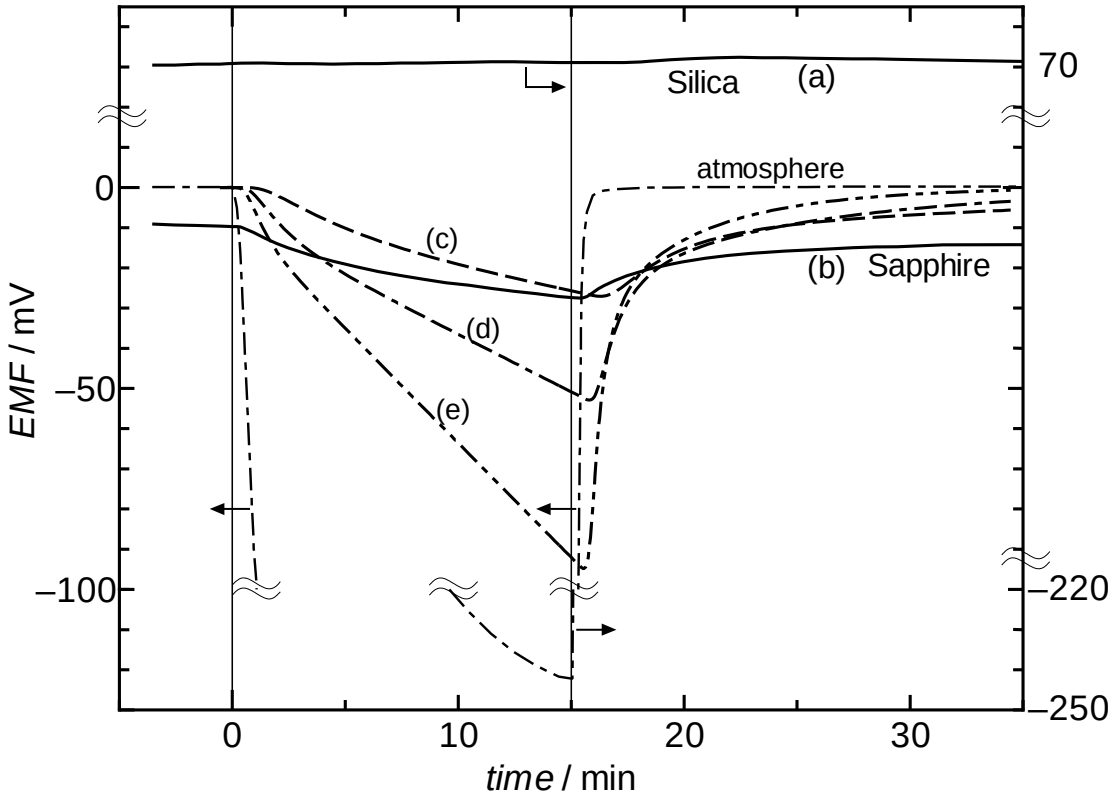

Fig. 3. Comparison of insulating materials for Pt electrode. (a): EMF change on Pt electrode with silica tube, (b): EMF change on Pt electrode with sapphire tube. The EMFs were measured in a $20Na_2O \cdot 10CaO \cdot 70SiO_2$ melt at 1200°C. The dot-dashed line shows the oxygen concentration change in the atmosphere. Curves (c) to (e) show simulated activity changes with diffusion coefficients of 2×10^{-4}, 5×10^{-4} and 1×10^{-3} cm^2s^{-1}, respectively.

no meaningful change. After the atmosphere was changed to air, the EMF value at the former electrode rose within 1 min while the value at the latter did not change. If the result on the former electrode is assumed to be true, O_2 diffusion should be very fast since the incubation time of EMF change was very short, about 30 seconds. Curves c to e in Fig. 3 show the simulated results with various diffusion coefficient values. The shape of curve c was different from that of experimental curve b; the calculated incubation time was much longer than in curve b. Curve e, having a shorter incubation time, showed a larger ΔE change. Moreover, the diffusion coefficient was 1×10^{-3} cm^2s^{-1}, which was extremely large compared with those in the literatures.[7, 29-31] For these reasons, the obtained values are not plausible. On the other hand, curve a, the result on the electrode with silica, showed no sign of O_2 diffusion within the experimental period. The difference between these electrodes was limited to the insulating materials. This phenomenon could be explained by the idea that alumina must have electronic conduction at the measuring temperature and that some redox reaction of oxygen occurred at the melt-air interface on the alumina. When an ordinary sintered alumina tube (SSA-S, Nikkato) was used instead of a sapphire single crystal, the result of short incubation time and large EMF change was the same. Hence, it was concluded that alumina cannot be used as the insulating material for oxygen diffusion measurement at high temperatures.

Figure 4 shows the oxygen activity change measured with the Pt electrode with silica. The *y* axis shows the oxygen activity calculated from equation (2). The Pt electrode was set at a depth of 4.5 mm from the surface in a melt 6 mm deep. The atmosphere was changed from dry air to N_2 and from N_2 to air. The EMF value began to decrease about 25 min after the change of atmosphere from air to N_2. After the atmosphere was changed from N_2 to air again, the EMF started to increase within about

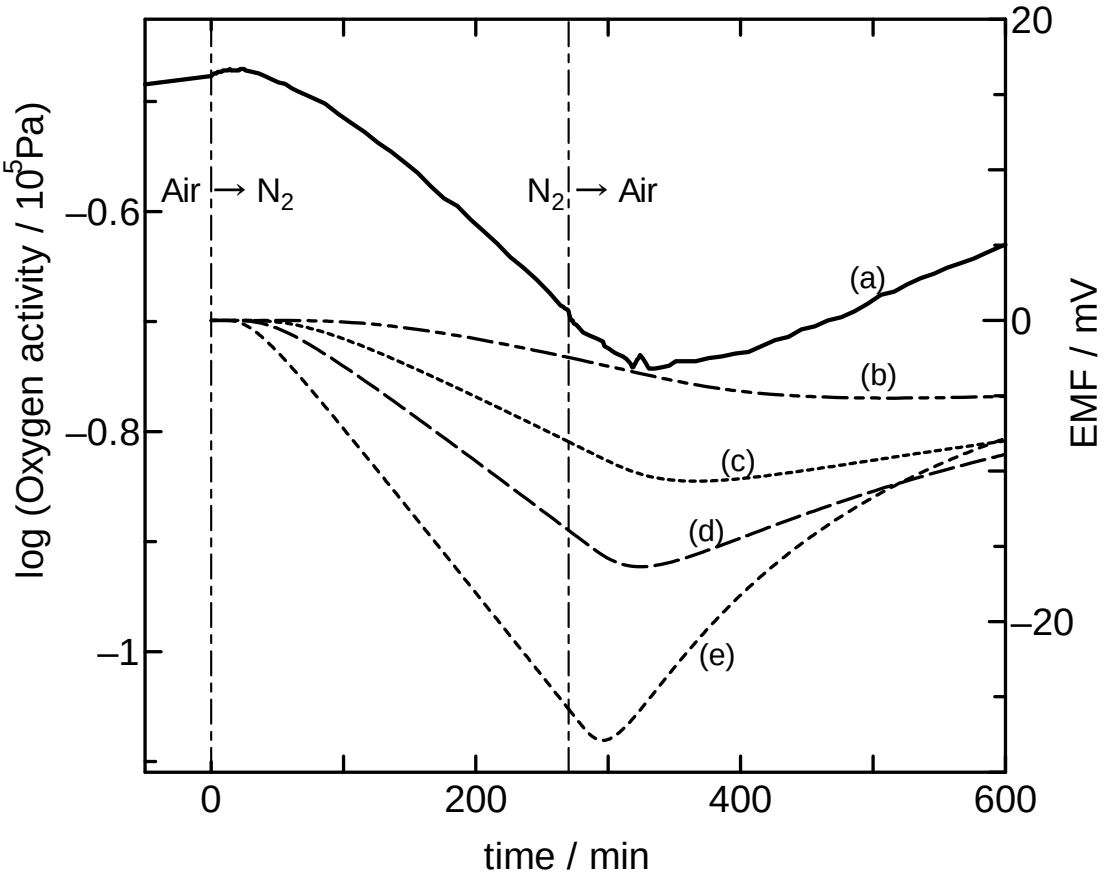

Fig. 4. Measured oxygen activity change with atmosphere change at 1200°C and simulated results. Curve (a) shows experimental results in $20Na_2O \cdot 10CaO \cdot 70SiO_2$ melt. Curves (b) to (e) show simulated activity changes with diffusion coefficients of 2×10^{-6}, 4×10^{-6}, 6×10^{-6}, and 1×10^{-5} cm^2s^{-1}, respectively. Melt depth was 6.5 mm and the electrode position was 4.5 mm from the surface.

50 min. The EMF value rose or dropped slightly just after the atmospheric change, and the direction of this change was opposite to the EMF change caused by oxygen diffusion. When the amount of air passed in the zirconia electrode as a reference gas was increased, the EMF change value just after the atmosphere change became smaller. If the inner pressure of zirconia electrode was lower than the outer one, this change was explained to be due to penetration of the atmosphere into the zirconia electrode through the alumina or zirconia cement of the electrode used.

At the beginning, the EMF should be 0 mV, and aO_2 the same as pO_2. The EMF value at $t = 0$ in Fig. 4 (a) was, however, about 16 mV. From equation (2), this means that the oxygen activity in the melt was higher than that in air. The activity change in this figure did not agree with the simulated result if the activity in the melt was very high at $t = 0$. The same phenomenon can be observed in Fig. 3, where the EMF on the silica electrode was +70 mV while that on the electrode covered with sapphire was –10 mV. This might be due to O^{2-} activity change on the electrode. A more precise equation than (2) can be written thus:

$$\Delta E = \frac{\mathrm{R}T}{4\mathrm{F}} \ln\left(\frac{a\mathrm{O}_{2\,\mathrm{Pt}}/(a\mathrm{O}^{2-}{}_{\mathrm{Pt}})^2}{p\mathrm{O}_{2\,\mathrm{Zr}}/(a\mathrm{O}^{2-}{}_{\mathrm{Zr}})^2} \right) \qquad (13)$$

where aO^{2-} is the activity of the oxide ion in the melt near the Pt or zirconia electrode. If aO^{2-} near the Pt electrode were different from that near the zirconia, ΔE would be non-zero even if $aO_2 = pO_2$. This would be caused by the basicity change from silica dissolution in the melt. Silica, used as the insulator on the Pt electrode, is soluble in melts, and must be concentrated near the electrode. Since the oxide ion is produced from Na_2O and CaO, silica dissolution will decrease the aO^{2-} and decrease the basicity. Hence, the ΔE value will rise from equation (13). This consideration means that an accurate oxygen activity value cannot be obtained with an electrode containing a soluble

silica insulator. If the basicity near the electrode were to change during the course of the measuring period, it would create an uncertainty factor for oxygen diffusion measurement. In order to reduce this problem, a shorter measurement period is desirable.

Simulated oxygen activity changes are also shown in Fig. 4 as curves b to e. Comparing the curves in this figure, the tendency of change in curve d was similar to the experimental result. Hence, the oxygen diffusion coefficient in the melt was around 6×10^{-6} cm^2s^{-1}. This value is not far from that of the previous literature.[7, 29-31]

Oxygen activity change was measured again in the other melt to confirm reproducibility. Figure 5 shows the result measured under similar conditions as in Fig. 4. Though curve d, calculated with the same diffusion coefficient of 6×10^{-6} cm^2s^{-1}, was the nearest to the experimental curve, the agreement of these curves were worse than in Fig. 4. These simulated curves were calculated under the assumption of ideal conditions in which the initial oxygen activity in the melt is the same as that in the atmosphere, and there is no reaction on the wall of alumina crucible. These assumptions are not always valid since it takes considerable time to attain uniform oxygen activity in the whole melt, and oxygen production or consumption on the wall inevitably occurs because of the slight electronic conductivity of alumina. In order to minimize these errors, the melt depth should not be large and the Pt electrode should be set away from the bottom and wall of the alumina crucible. In this cell design, the shallow melt depth compared with the melt surface area might cause convection, which creates a larger apparent diffusion coefficient. The Pt electrode position is another potential error factor. If the Pt plate is uneven or tilted, the shallow part of the plate in the melt detects the oxygen diffusion more quickly and inflates the apparent diffusion coefficient. Though a deeper electrode position and a deeper cell minimize this error because of a smaller relative position

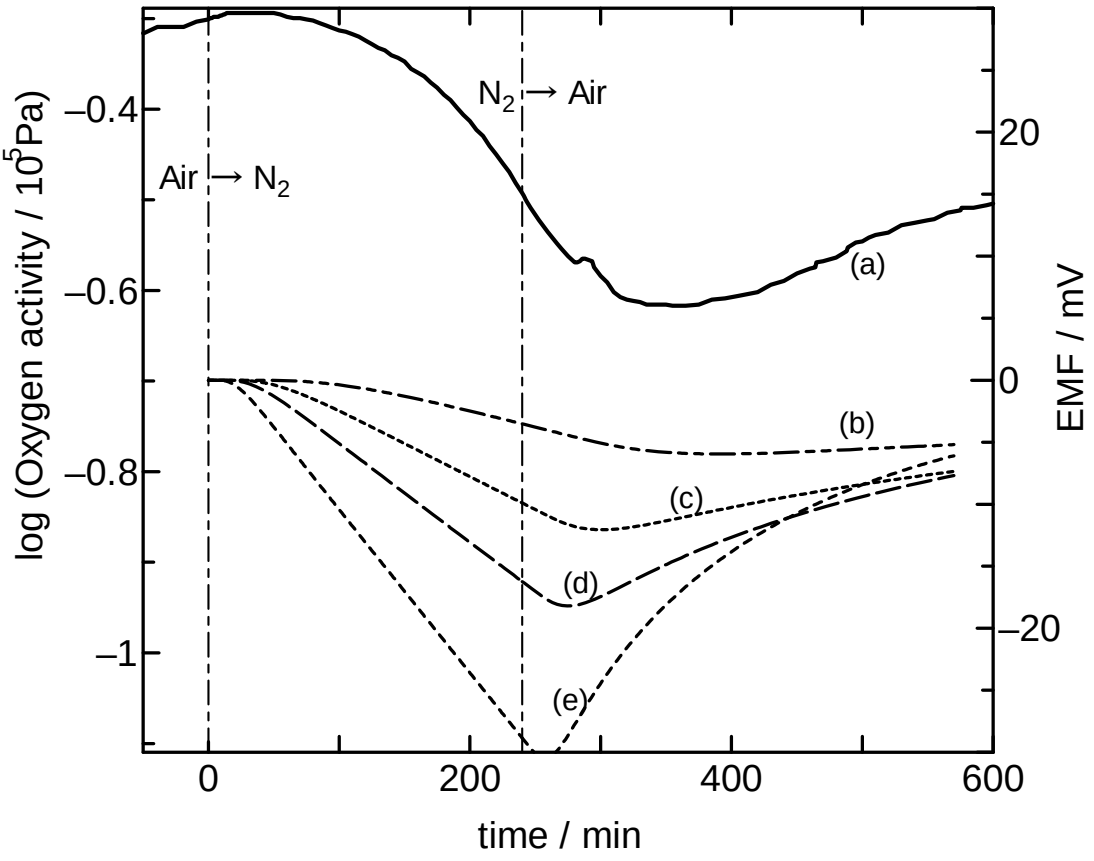

Fig. 5. Reproducibility of the oxygen activity change. The glass composition and temperature of (a) are the same as those in Fig. 4; the diffusion coefficients for (b) through (e) also match those of Fig. 4. Melt depth was 6 mm and the electrode position was 4 mm from the surface in this case.

error, adoption of this condition is not advised because of the reason mentioned above. If there is a material with no electronic conductivity and high corrosion resistance, cell design can be changed and the Pt electrode can be set at a bottom of the crucible. Then, it will be possible to determine the oxygen diffusion coefficient more accurately.

Figure 6 shows a result of oxygen diffusion in a melt with Sb_2O_3. Though a diffusion coefficient of 4×10^{-6} cm^2s^{-1}, a similar value as that in the melt without Sb_2O_3, resulted in better agreement, the similarity between the measured and the calculated curves was still not good. The reason for the low accuracy was due to the small EMF change caused by the buffer effect of the polyvalent element and the errors mentioned above. In order to determine the solubility of oxygen and the reaction rate between oxygen and the element, a more accurate procedure is needed.

4-5 Conclusion

The EMF method for a measurement of oxygen diffusion coefficient was examined using oxygen concentration change in the atmosphere. The following results were obtained.

The material covering the Pt lead of the electrode at the interface between the melt and the atmosphere should be an electronic insulator. When alumina was used, an extremely large apparent oxygen diffusion was observed, presumably caused by the slight electronic conductivity in alumina. Hence, it was concluded that alumina cannot be used for the insulator. Silica could be used for the insulator since no redox reaction was observed at the silica surface. Silica, however, proved to be soluble in the melt and caused high apparent oxygen activity, probably because of decreased basicity near the electrode.

The oxygen diffusion coefficient was estimated by comparing the EMF change

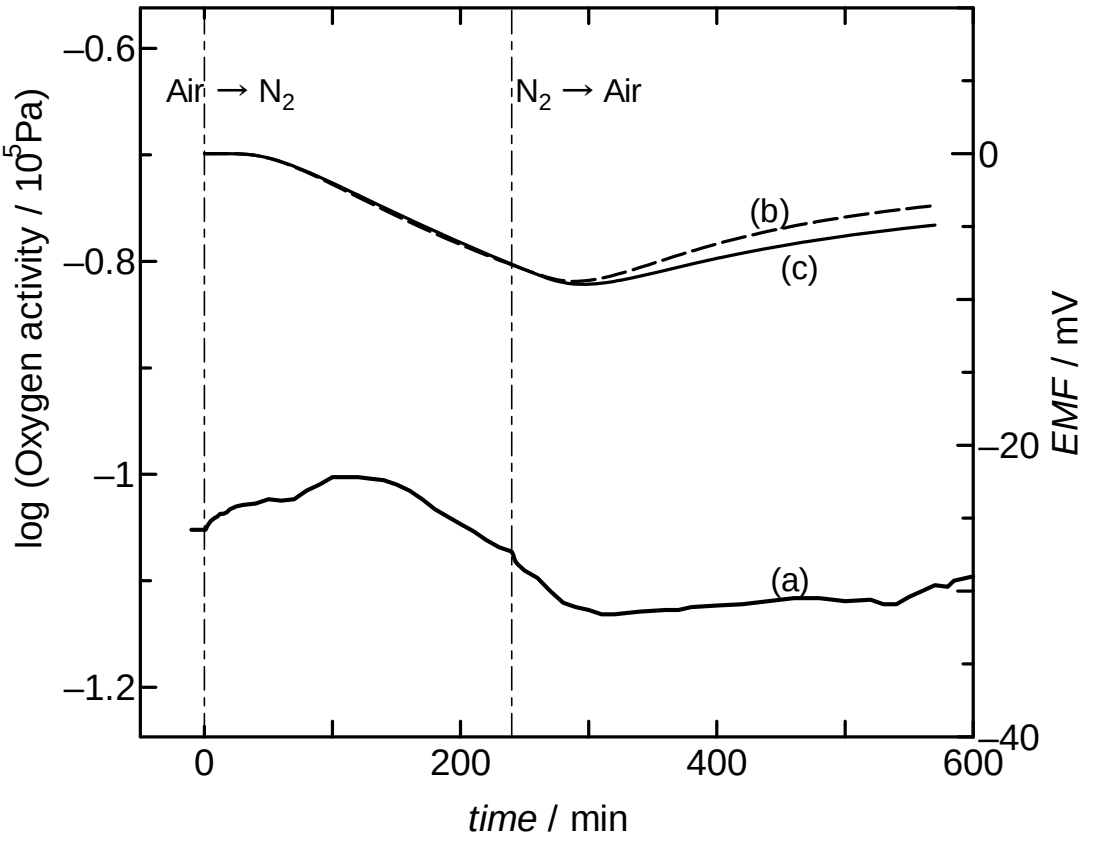

Fig. 6. The oxygen activity change in $20Na_2O \cdot 10CaO \cdot 70SiO_2 + 1Sb_2O_3$ melt at 1200°C. Curve (a) is the measured result. Curves (b) and (c) were both calculated under the assumptions that the oxygen diffusion coefficient is 4×10^{-6} cm^2s^{-1}, and the half wave potential of Sb, $E^{1/2}$, is +100 mV vs. air as a reference gas, in which case, $[Sb^{5+}]/[Sb^{3+}]$ = 0.2 if $aO_2 = 0.2$. $[O_2]_{satd.}$ was 0.01 $molL^{-1}$ for (b) and 1 $molL^{-1}$ for (c); k_b was 8×10^{-7} for (b) and 2×10^{-4} for (c). Melt depth was 8 mm and the electrode position was 4 mm from the surface.

with simulated curves. The oxygen concentration profile was numerically calculated with Fick's law, and a curve of the concentration change at various depths was obtained. From the comparison, the diffusion coefficient was 6×10^{-6} cm^2s^{-1} in a $20Na_2O\cdot10CaO\cdot70SiO_2$ melt at 1200^oC. Convection in the melt or unevenness of the electrode plate results in a larger apparent diffusion coefficient. In a melt containing Sb_2O_3, the agreement of measured and calculated EMF change curves was not good because of the low accuracy and small EMF change.

Reference

1. S. M. Budd, V. H. Exelby and J. J. Kirwan, *Glass Technol.*, **3**, 124-129 (1962).
2. T. J. Harper, *Glass Technol*., **3**, 171-175 (1962).
3. H. O. Mulfinger, *J. Am. Ceram. Soc.*, **49**, 462-467 (1966).
4. M. L. Pearce, *J. Am. Ceram. Soc.*, **47**, 342-347 (1964).
5. M. C. Weinberg, P. A. Kondos and R. S. Subramanian, *Glass Technol.*, **31**, 72-76 (1990).
6. R. G. C. Beerkens, *Glastech. Ber. Glass Sci. Techn.*, **68**, 369-380 (1995).
7. Doremus, *J. Am. Ceram. Soc.*, **43**(**12**), 655-661 (1960).
8. P. S. Esptein and M. S. Plesset, *J. Chem. Phys.*, **18**(**11**), 1505-1509 (1950).
9. M. Cable and D. J.Evans, *J. Appl. Phys.*, **38**(**7**), 2899-2906 (1967).
10. M. C. Weinberg, P. I. K. Onorato and D. R. Uhlmann, *J. Am. Ceram. Soc.*, **63**(**3-4**), 175-180 (1980).
11. L. Nêmec, *Glass Technol.*, **15**(**6**), 153-156 (1974).
12. R. S. Subramanian and B. Chi, *Chem. Eng. Sci.*, **35**, 2185-2194 (1980).
13. H. Hübenthal and G. H. Frischat, *Glastech. Ber.*, **60**(**1**), 1-10 (1987).
14. H. Yoshikawa and Y. Kawase, *Glastech. Ber. Glass Sci. Techn.*, **70**(**2**), 31-40 (1997).
15. H. Yoshikawa, H. Miura and Y. Kawase, *J. Mater. Sci.*, **33**, 2701-2707 (1998).
16. R. Terai and Y. Oishi, *Glastech. Ber.*, **50**(**4**), 68-73 (1977).
17. H. Yinnon and A. R. Cooper Jr, *Phys. Chem. Glasses*, **21**(**6**), 204-211 (1980).
18. T. Tran and M. P. Brungs, *Phys. Chem. Glasses*, **21**, 178-183 (1980).
19. H. A. Schaeffer, T. Frey, I. Löh and F. G. K. Baucke, *J. Non-Cryst. Solids*, **49**, 179-188 (1982).
20. V. A. Lenhart and H. A. Schaeffer, *Glastech. Ber.*, **58**, 139-147 (1985).

21. M. Sasabe and K. S. Goto, *Metall. Trans.*, **5**, 2225-2233 (1974).

22. J. P. Hilger and O. Lafroukhi, *Glastech. Ber.*, **64**, 299-304 (1991).

23. J. Crank, The mathematics of diffusion, Clarendon Press, Oxford. (1956).

24. R. G. C. Beerkens and H. Waal, *J. Am. Ceram. Soc.*, **73**, 1857-1861 (1990).

25. K. Takahashi and Y. Miura, *J. Non-Cryst. Solids*, **38&39**, 527-532 (1980).

26. C. Rüssel, *J. Non-Cryst. Solids*, **134**, 169-175 (1991).

27. G. Gönna and C. Rüssel, *J. Non-Cryst. Solids*, **261**, 204-210 (2000).

28. G. Gönna and C. Rüssel, *J. Non-Cryst. Solids*, **272**, 139-146 (2000).

29. H. D. Schreiber, S. J. Kozak, A. L. Fritchman, D. S. Goldman and H. A. Schaeffer, *Phys. Chem. Glasses.*, **27**, 152-177 (1986).

30. W. N. Lawless and B. Wedding, *J. Appl. Phys.*, **41**, 1926-1929 (1970).

31. D. S. Goldman and P. K. Gupta, *J. Am. Ceram. Soc.*, **66**, 188-190 (1983).

Chapter 5. Measurement of the surface tension of glass melts.

5-1 Introduction

The surface tension of glass melts is one of the most important properties relating to the refining[1] and homogenization of melts. It is also important in simulation of glass manufacturing since it affects the formation and extinction of bubbles in melt. Surface tension has been measured in several silicate[2-6] and borosilicate[7] melts. In silicate melts, the surface tension is about 300 $mN \cdot m^{-1}$ and temperature has only a small effect.[2,4] For borate, it is about 200 $mN \cdot m^{-1}$ and shows a stronger temperature dependence[7]. It is known that surface tension is one of the properties which is subject to the additivity rule of its components, as are density[8] and thermal expansion.[9] Recently, Kucuk et al.[10] proposed parameters of surface tension for the components of glass melts after summarizing parameters from several other authors. However, there are some discrepancies in their data.

There are several methods for measuring surface tension. For glass melts, the sessile drop method,[3,5-7] the pendant drop method,[5,11] the ring method[12] and the maximum bubble pressure method[2-4] have been used. The sessile drop and pendant drop provide accurate data because they are static methods and the results are thus unaffected by resistance from the viscous flow. However, it is essential to have precise data about the drop shape of the liquid which have high surface tension and density such as glass melts.[13] Data collection became easier with the development of image capturing techniques and computer systems. A major problem for the drop methods as well as for the ring method is changes in the surface composition by volatilization from the surface during measurement. Moreover, for these methods, the substrate material and atmosphere are limited since low wettability is required. Contamination of the surface by the reaction between the substrate and the melt is another problem that has ramifications for these static methods since the drop is not renewed.

The problem of contamination is not severe for the maximum bubble pressure method compared to the static methods, since the air volume inside the bubble is small and the interface is refreshed for each bubble formation. Another advantage of the maximum bubble pressure method is that the measurement technique is simple: we measure only the pressure difference between internal bubble pressure and the atmosphere for the bubble formed at the tip of a capillary, which grows with increasing pressure and expands until it suddenly breaks. Under this method, the differential pressure, ΔP, is expressed as

$$\Delta P = \rho g h + 2\sigma / r, \qquad (1)$$

where ρ is the density of the melt, g is the gravity constant, h is the depth of the tip below the surface of the melt, σ is the surface tension and r is the radius of bubble. ΔP increases and r decreases as the gas is introduced into the capillary, as shown in Fig. 1a, reaching its maximum at time $t = t_{max}$ when r becomes the size of the capillary radius, that is, when r is the smallest. The introduction of more gas results in a larger bubble, which leads to a longer radius, which in turn causes a decrease in ΔP according to Eq. (1). The bubble then expands quickly, as shown in Fig. 1a, and is released from the capillary.

It is critical under the maximum bubble pressure method that the shape and size of the capillary be determined precisely and that the gas flow rate be controlled carefully to avoid any influence of excess pressure caused by viscous flow. The latter requirement is especially difficult to satisfy for viscous liquids such as glass melts. Therefore, to the best of our knowledge, although this method has been applied to slags,[14] it has been applied to glass melts only once since Bradley's study in 1938,[3] in a study by Akhtar and Cable in 1968.[4]

Another experimental problem arises from the wettability of capillary material

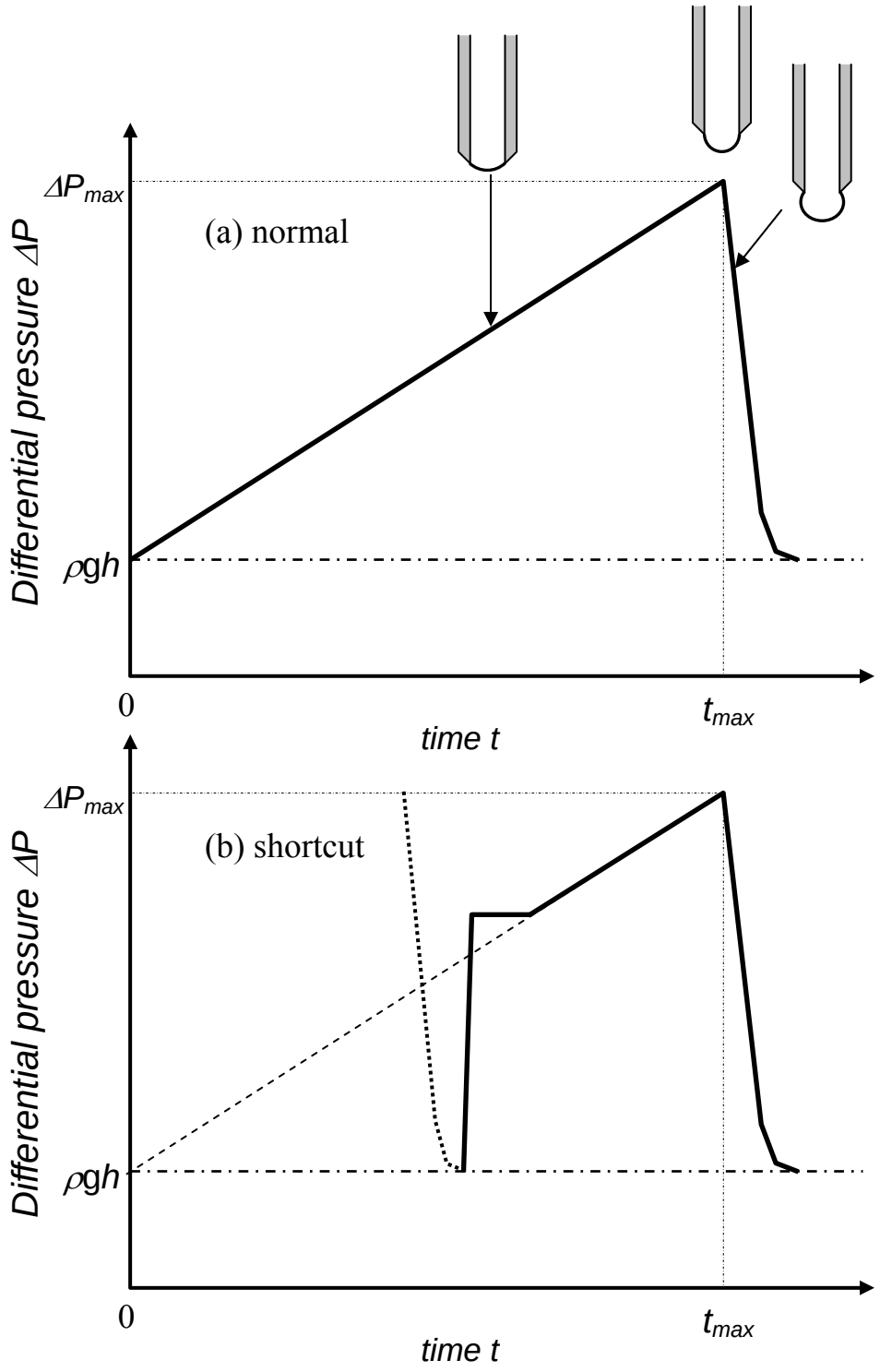

Fig. 1. Comparison of the normal (a) and shortcut (b) methods. Bubble shapes at certain points are also shown. Differential pressure rises with time and decreases sharply after the maximum point.

with melt. If wettability is high, the melt will rise in the capillary at the beginning of bubble formation because of the capillary action, which might change the effective inner diameter of the capillary. On the other hand, if wettability is too low and the capillary tip does not have a thin, sharp edge, it is not clear what radius value should be used since bubble diameter would change before a perfect hemisphere is formed.

In the present study, the effects of capillary material and shape were examined with respect to bubble-forming time. We then applied the maximum bubble pressure method was applied to several glass melts including volatile borosilicate glass.

5-2 Experimental

Three types of platinum tubes were used to form bubbles in glass melts, as

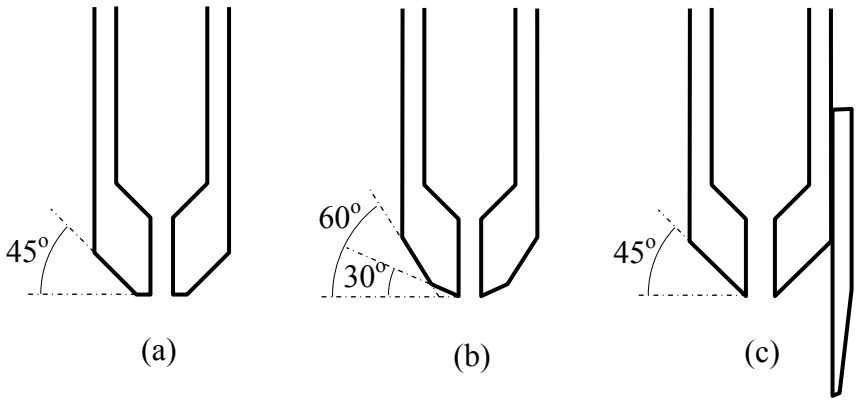

Fig. 2. Shapes of the tips of the tubes used for surface tension measurement. The materials used in the tips are (a) Pt-20%Rh, (b) zirconia-dispersed Pt-5%Au and (c) zirconia-dispersed Pt-10%Rh with a needle made of zirconia-dispersed Pt-5%Au attached the tip.

shown in Fig. 2. The outer diameter of each tube was 6 mm and the diameter of the hole at the tip of tube was 1.0 or 1.5 mm. The diameters of the holes were measured with a microscope with a scale. The tubes were made of Pt-20%Rh (Fig. 2a), zirconia-dispersed Pt-5%Au (FKS Pt-5%Au, Furuya Metal) (Fig. 2b) and zirconia-dispersed Pt-10%Rh (FKS Pt-10%Rh, Furuya Metal) (Fig. 2c). The tips of the tubes were cut to 45^{o} but flat near the hole (Fig. 2a), to 30^{o} at the outer side and 60^{o} near the hole (Fig. 2b), and to 45^{o} for (Fig. 2c), respectively. The holes were slightly distorted circles with radii of 0.486±0.010 mm for (a), 0.534±0.010 mm for (b) and 0.768±0.010 mm for (c). Tube (c) was equipped with a needle made of FKS Pt-5%Au, which was attached beside the tip.

The configuration of the measuring apparatus is shown in Fig. 3. The tube was connected to a gas line through a micro valve and to a digital manometer (DP-200A, Okano Works, Ltd.) and was introduced into an electric furnace. Dry air (N_2 80% - O_2 20%) was used as a bubble-forming gas. The manometer had a measuring range of 0 to 2000 Pa with an error limit of 0.2% and a response time of 0.02 sec. A platinum crucible was set in the furnace. An alumina cover with a hole was placed over the crucible to avoid contamination by dust from the upper hole of the furnace. After the temperature was raised to the measuring point, the tube was moved down toward the melt in units of 0.02 mm using a screw with scale. Contact between the glass melt and the tip of the tube was detected electrically using an impedance meter (hp 4262A LCR meter, Hewlett Packard). A small amount of dry air was introduced into the tube at a rate of approximately 5×10^{-4} cm^3s^{-1} and a rise in pressure was confirmed at the time of contact. The tube was then moved down slowly to a predetermined position and the bubble generation rate was adjusted with a mass flow controller and a micro valve. The rate of gas flow ranged from 2×10^{-4} cm^3s^{-1} to 5×10^{-2} cm^3s^{-1}. The difference in pressure

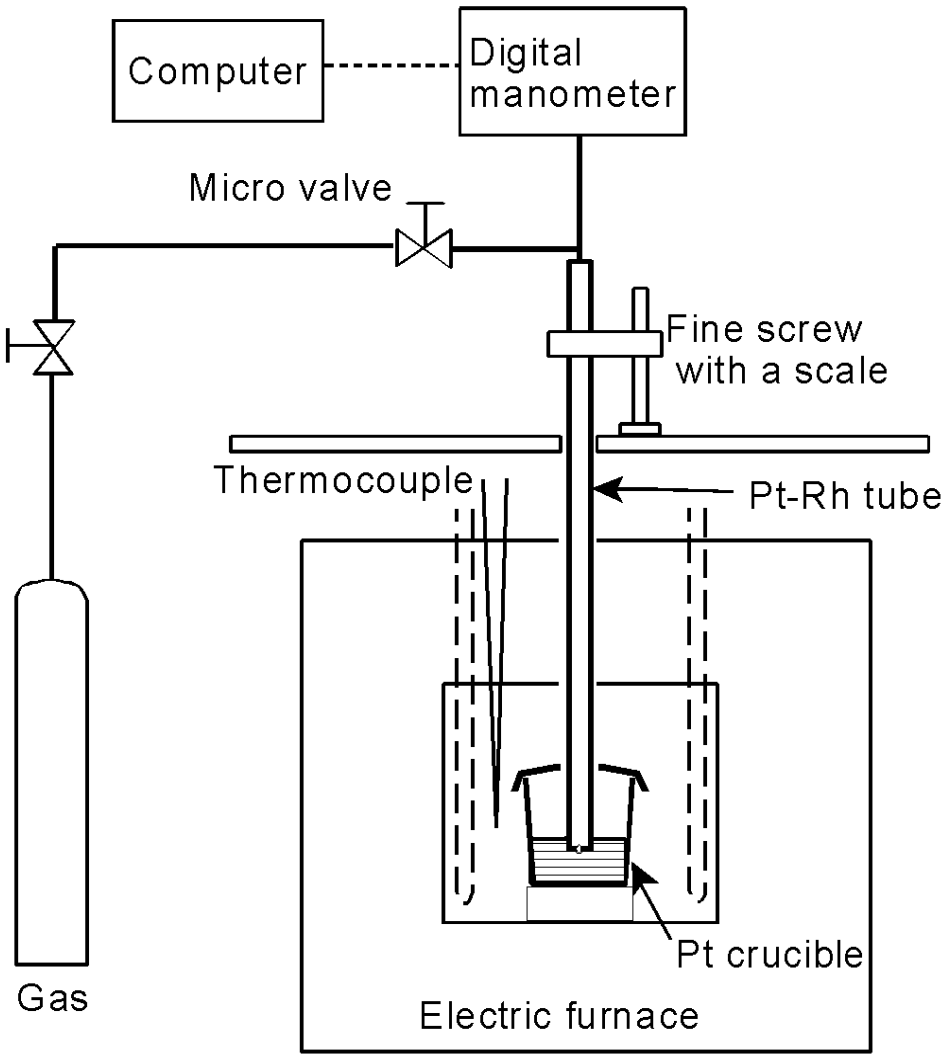

Fig. 3. Illustration of surface tension measurement in glass melt by the maximum bubble pressure method. Gas is introduced in the melt through the micro bulb and the pressure inside the tube is measured by the digital manometer.

between the inside of the tube and the atmosphere was recorded on a chart recorder or stored in a computer, allowing measurement of the maximum differential pressure ΔP_{max} and bubble-forming time. The differential pressure rose when the gas supply was started, reached its maximum when the bubble radius became identical to the tube radius, r_0, then decreased drastically, as shown in Fig. 1a. When the bubble generation rate was slower than 0.2 min^{-1}, a shortcut method was adopted to save experimental time. Under the shortcut method, gas was first supplied at two-thirds of the amount needed to achieve the maximum differential pressure in about 5 sec, and then it was supplied at a normal rate. In this case, t_{max} was determined by extrapolation of the rising pressure profile, as shown in Fig. 1b.

The surface tension σ was determined using the equation

$$\sigma = c \cdot r_0(\Delta P_{max} - \rho g h) / 2 \qquad (2)$$

where r_0 is the radius of the Pt capillary, which was corrected for the thermal expansion of Pt and c is the bubble-shape correction factor, which is smaller than unity. This factor is a function of r_0, ρ and σ and was calculated using the data reported by Sugden.[15] Since r_0 was small and the surface tension was high, the correction factors were determined to range from 0.99 to 0.995.

Because of the thermal expansions of the melt and Pt tube, the depth h, which is nominally 5 mm by the scale, could change with temperature. In order to calibrate h, a glassy carbon tip or an FKS Pt-5%Au tip, both of which are less wettable by the melt, was attached to the Pt tube at its end with a platinum wire. The position of the surface was checked at each temperature using the electrical contact method. The glassy carbon tip was used in an N_2 atmosphere. Reproducibility of the surface position was within 0.3 mm against the heating and cooling cycle, which corresponded to a maximum of 0.6% of error. When tube type (c) was used, the melt surface position was checked at

Table 1. Composition of the glasses in mol%. Green float contains 0.2mol% Fe_2O_3 and 0.04mol% of TiO_2.

	SiO_2	Al_2O_3	B_2O_3	Na_2O	K_2O	MgO	CaO	SrO
Soda-lime	70.0			20.0			10.0	
ONRI. Std.	71.7	1.1		12.7	0.3	3.3	10.9	
Green float	70.4	0.9		12.8	0.4	5.8	9.4	
7740(pyrex)	83.3	1.4	11.3	4.0	0.02			
Non-alkali	66.1	11.3	7.6	<0.1		5.4	4.5	5.1
Soda borate			66.7	33.3				

each temperature with the FKS Pt-5%Au needle attached to the tube and more accurate values were obtained. Experimental error was estimated with NaCl melt with tube (c). The value was 1.5% lower than that reported in the literature[16] at 900°C and 0.7% higher at 1000°C.

Three kinds of soda-lime silicate glasses (simple soda lime, ONRI. Standard, Green float), borosilicate glass (7740, Pyrex), Asahi Non-alkali aluminoborosilicate glass and soda-borate glass were used for measurement. Their compositions are shown in Table 1.

5-3 Results

Figure 4 shows the relationship between bubble-forming time and the maximum differential pressure for the $20Na_2O$-10CaO-$70SiO_2$ glass melt at 1199°C measured with the Pt-20%Rh tip (a). The figure also compares the shortcut and normal methods. The x axis is the square root of the rate of bubble formation ($t_{max}^{-1/2}$), which was used in surface tension measurements in colloidal solution.[17,18] The data obtained

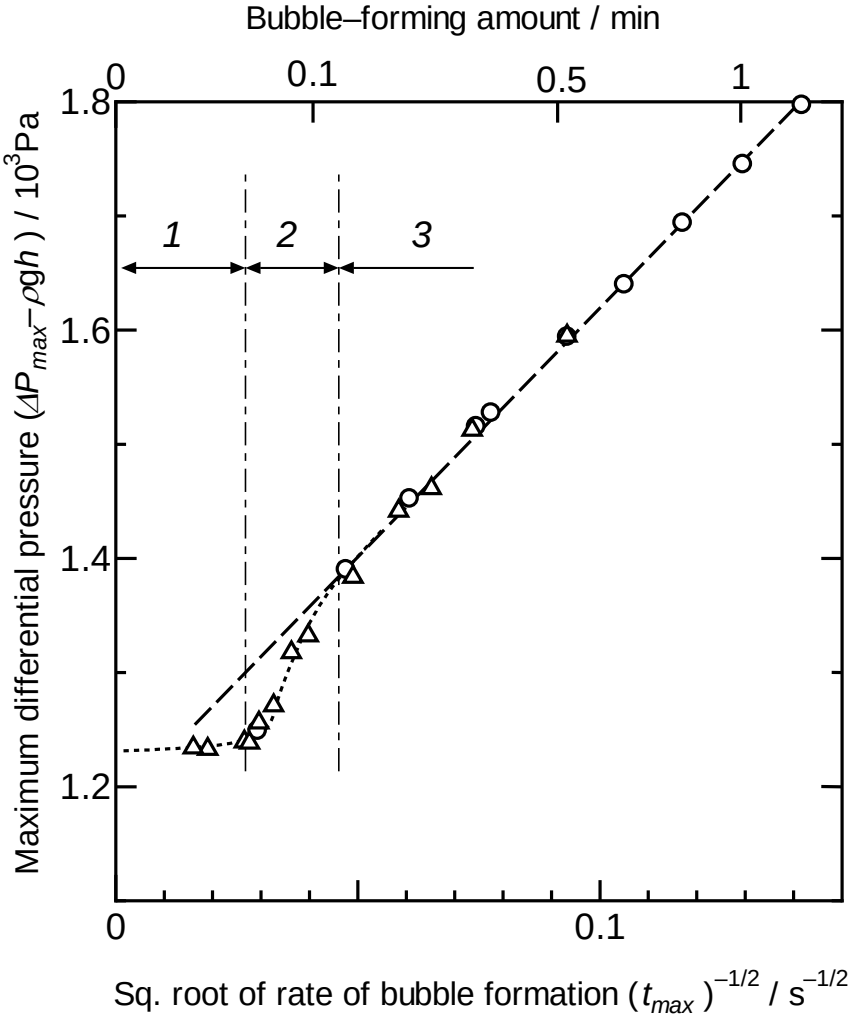

Fig. 4. Relationship between the bubble-forming time t_{max} and the maximum differential pressure ΔP_{max}, and comparison of values for the shortcut (△) and normal (○) methods. The graph is divided into three regions based on the dependence of ΔP_{max} on t_{max}.

by the shortcut method (△) agreed with that obtained by normal method (○) in this case; hence, the shortcut method was confirmed to be appropriate in the case of long bubble-forming time t_{max}. However, this does not hold for a short t_{max} due to the viscosity of the glass, as discussed below. The pressure – t_{max} curve shown in Fig. 4 can be classified into three regions. In Region 1, where the $t_{max}^{-1/2}$ is less than 0.02 (t_{max} > 2500 sec), the slope of the line is small and the static value of σ could be calculated by extrapolating the ΔP_{max} curve to the value at $t_{max}^{-1/2} = 0$; this region was the most important one for the surface tension measurement. In Region 2, the slope is much steeper, and in Region 3, where the square root of bubble-formation rate was greater than 0.05, the maximum pressure increased proportionally to $t_{max}^{-1/2}$, which was similar to the results obtained with colloid solutions.[17,18]

Figure 5 shows the ΔP_{max} value at various temperatures in $20Na_2O$-10CaO-$70SiO_2$ glass melt. At high temperatures, where the viscosity of the melt decreases, Region 1 becomes wider and the static σ_s value can easily be obtained. Additionally, the slope for the short t_{max} region is smaller at higher temperatures than at lower temperatures.

Figure 6 shows the ΔP_{max} value for the same glass as in Fig. 5 but measured using tip (b); there are some differences between these results and those shown in Fig. 5, though the general trends are similar. The surface tension values calculated with Eq. (2) were a little higher in Fig. 6 and Region 1 was wider than in Fig. 5. It is possible that the wetting of the tip by the melt had some effect on the results.

As shown in Fig. 7, the shortcut method gave a wider Region 1 than the normal method. Under the shortcut method, pressure inside the tube was raised quickly to two-thirds of the maximum value by introducing a large amount of gas. After maintaining this pressure for one minute, the gas was introduced again at the appropriate rate for

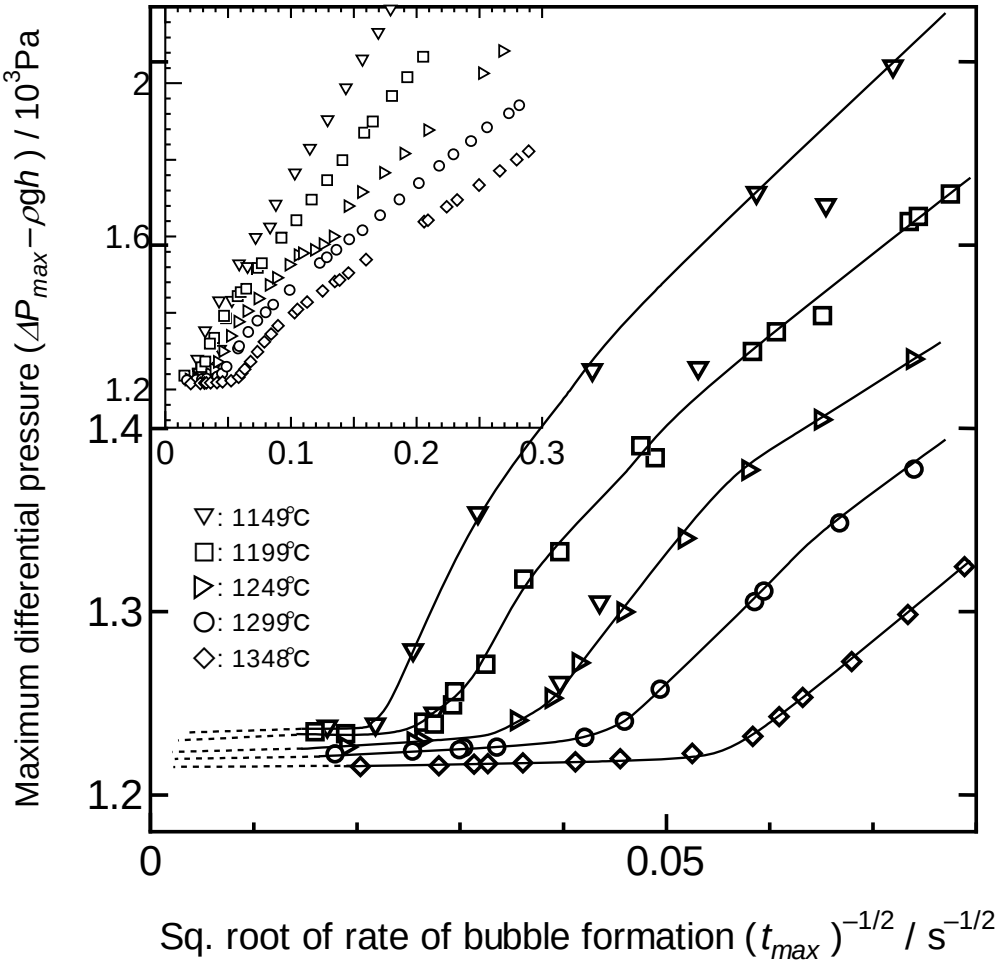

Fig. 5. Relationship between the maximum differential pressure ΔP_{max} and $t_{max}^{-1/2}$ in Regions 1 and 2. The melt composition was $20Na_2O$-10CaO-$70SiO_2$ and tip (a) was used. The insert shows the relationship over a wider range of t_{max} values.

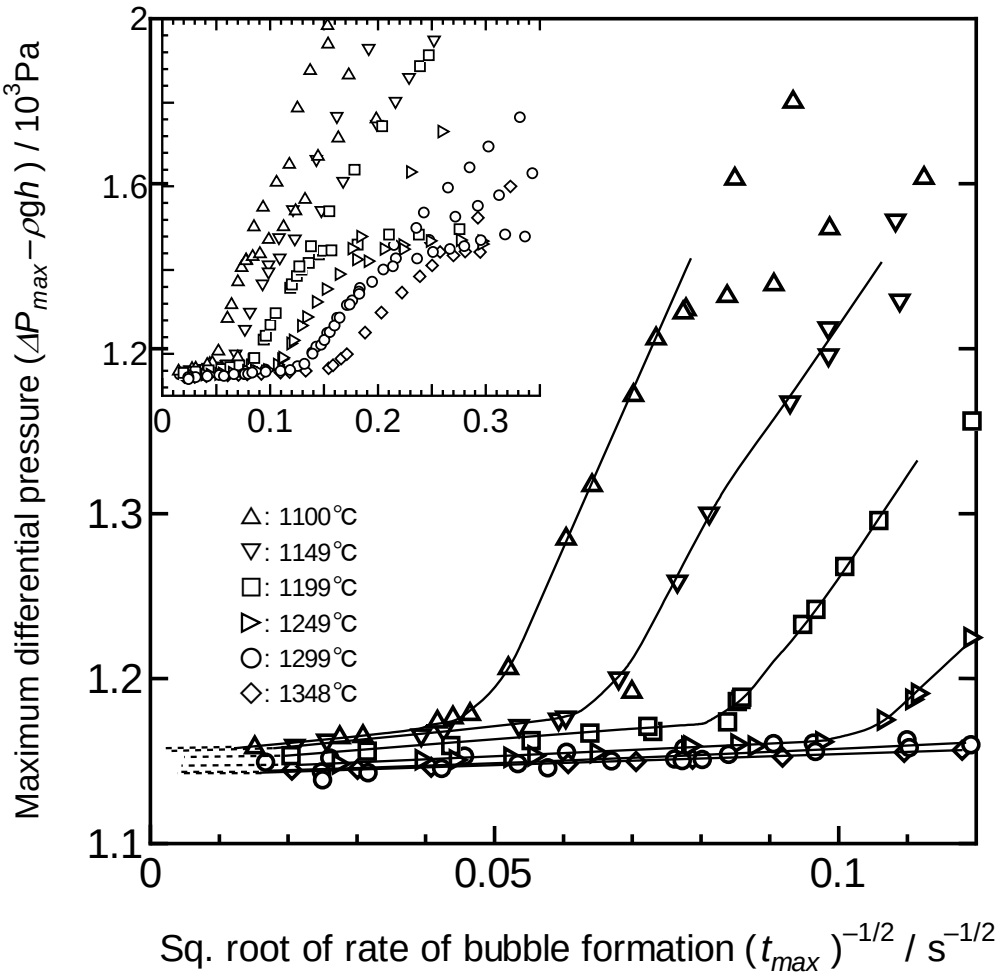

Fig. 6. Relationship between the maximum differential pressure ΔP_{max} and $t_{max}^{-1/2}$ in the Regions 1 and 2 obtained using tip (b). The melt was the same as that used in Fig. 5. The insert shows the relationship over a wider range of t_{max} values.

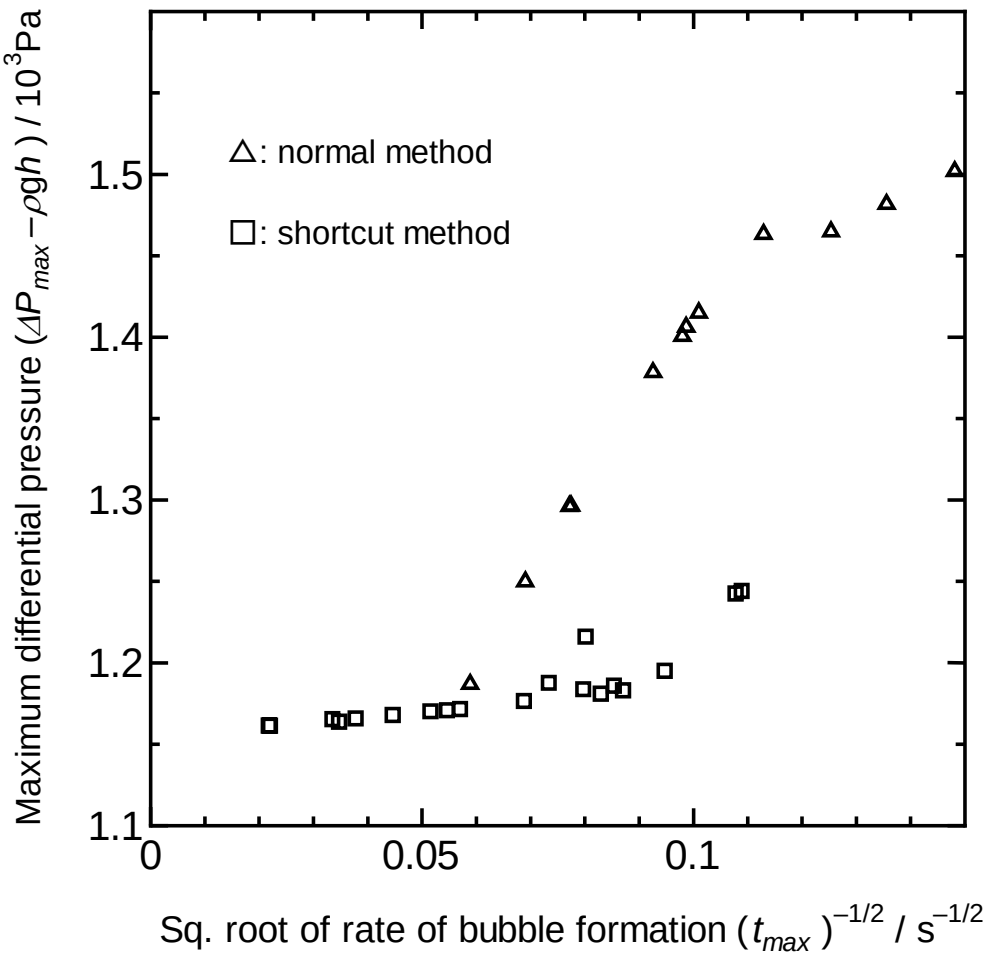

Fig. 7. ΔP_{max} values determined by the continuous normal method and the shortcut method in Regions 1 and 2. Region 1 was wider under the shortcut method.

bubble expansion. The effective bubble-forming rate was estimated from the rate at which the pressure rose after this pause. The increased width of Region 1 under the shortcut method is attributed to the following phenomena. When the tube is immersed in a melt, the melt rises into the tube by capillary action and adheres to the inside wall of the tube, reducing the effective hole diameter during bubble formation. This affects the measurements and decreases Region 1. However, a quick increase in pressure would avoid capillary rise of a viscose melt and the remaining melt in the tube could be purged during the pause and slow introduction of gas.

Since the shortcut method produced a wider Region 1, we adopted this method for all further experiments in the present study. This procedure was also advantageous in that it shortened the experimental period, which in turn was effective in reducing the composition change from volatilization.

The results for green float glass measured with tube (b) are shown in Fig. 8. When tube (a) was used, Region 1 became narrower, as was observed for the $20Na_2O$-$10CaO$-$70SiO_2$ melt in Fig. 5. The results for the 7740 and non-alkali glass melts measured with tube (c) are shown in Figs. 9 and 10, respectively.

Figure 11 shows the temperature dependence of surface tension determined for several glass melts. For the soda-borate melt, the results were consistent with the values reported in the literature.[7] For the soda-lime composition, the data obtained by Badger et al.[2] are also shown in this figure with a straight line. The unique behavior of the 7740 melt is obvious in Fig. 11. The surface tension showed a clearly positive temperature dependence, in contrast to the surface tension of other silicate glass melts. When we used tube (b) for the measurements for 7740, we obtained results similar to the data shown in Fig. 11, which were obtained with tube (c).

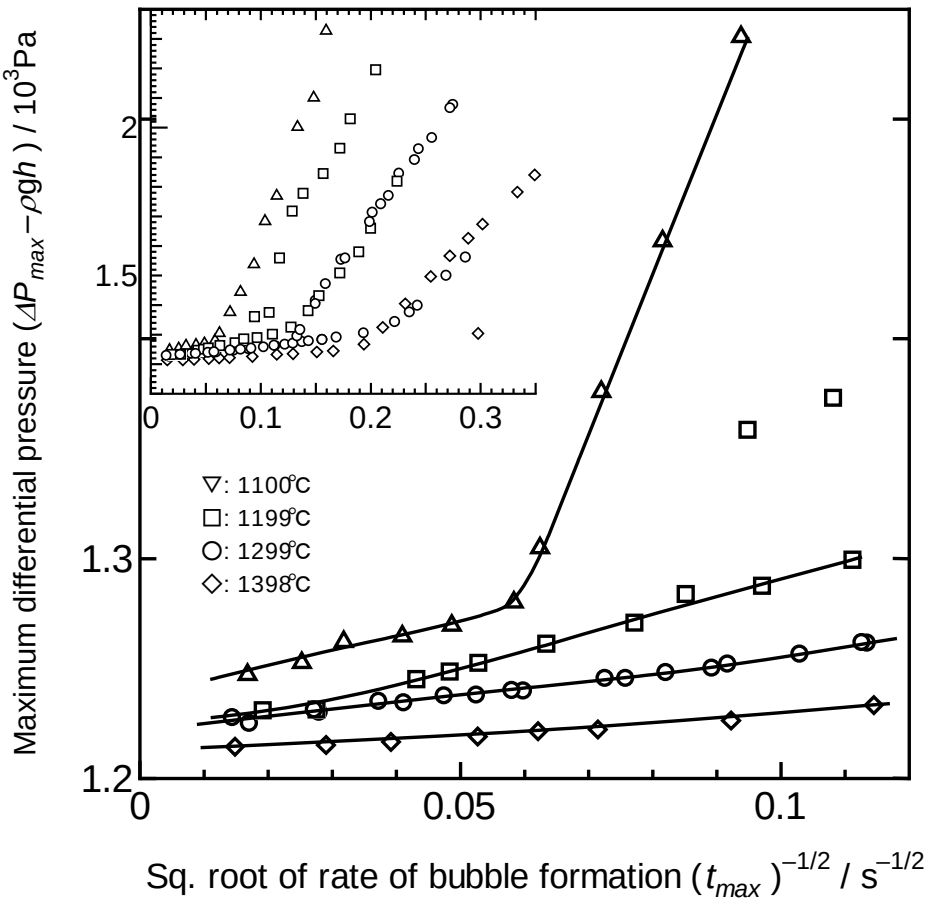

Fig. 8. Maximum differential pressure ΔP_{max} vs. $t_{max}^{-1/2}$ in Regions 1 and 2 for green float glass measured with tip (b). The insert shows the relationship over a wider range of t_{max} values.

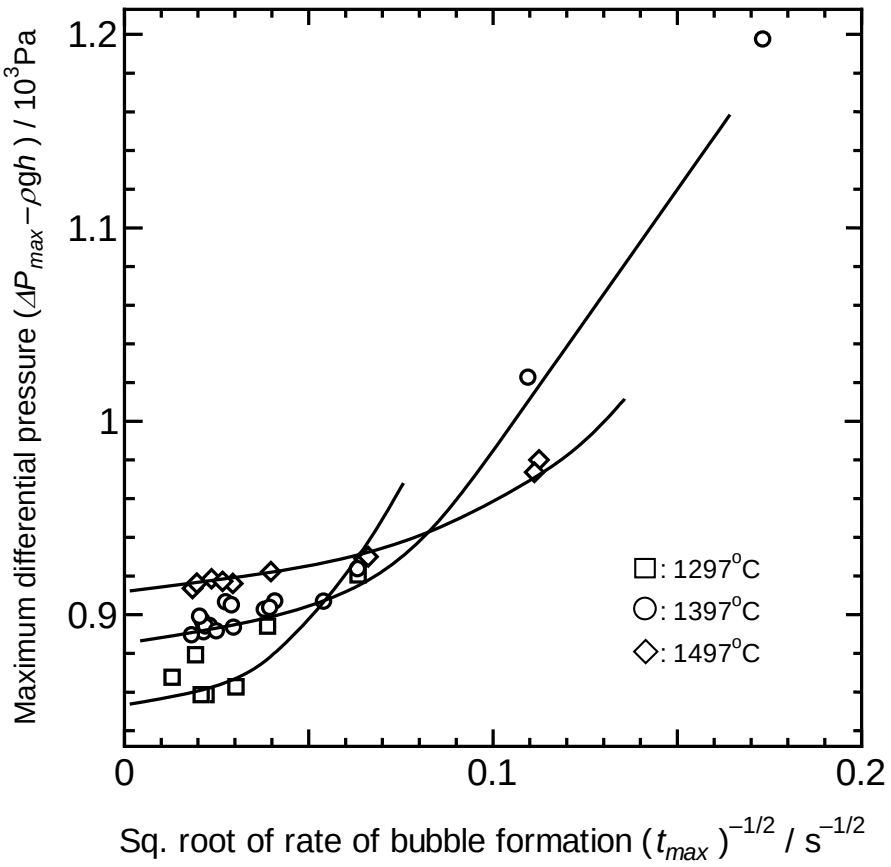

Fig. 9. Maximum differential pressure ΔP_{max} vs. $t_{max}^{-1/2}$ for the 7740 borosilicate melt measured with tip (c).

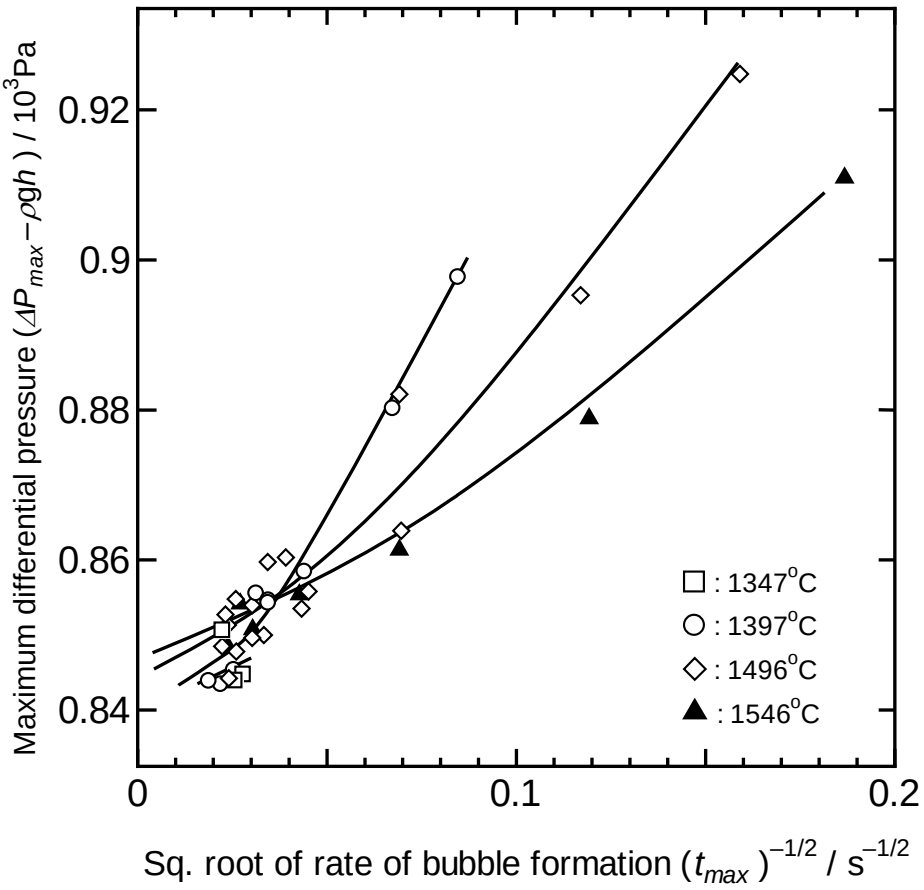

Fig. 10. Maximum differential pressure ΔP_{max} vs. $t_{max}^{-1/2}$ for the non-alkali glass melt measured with tip (c).

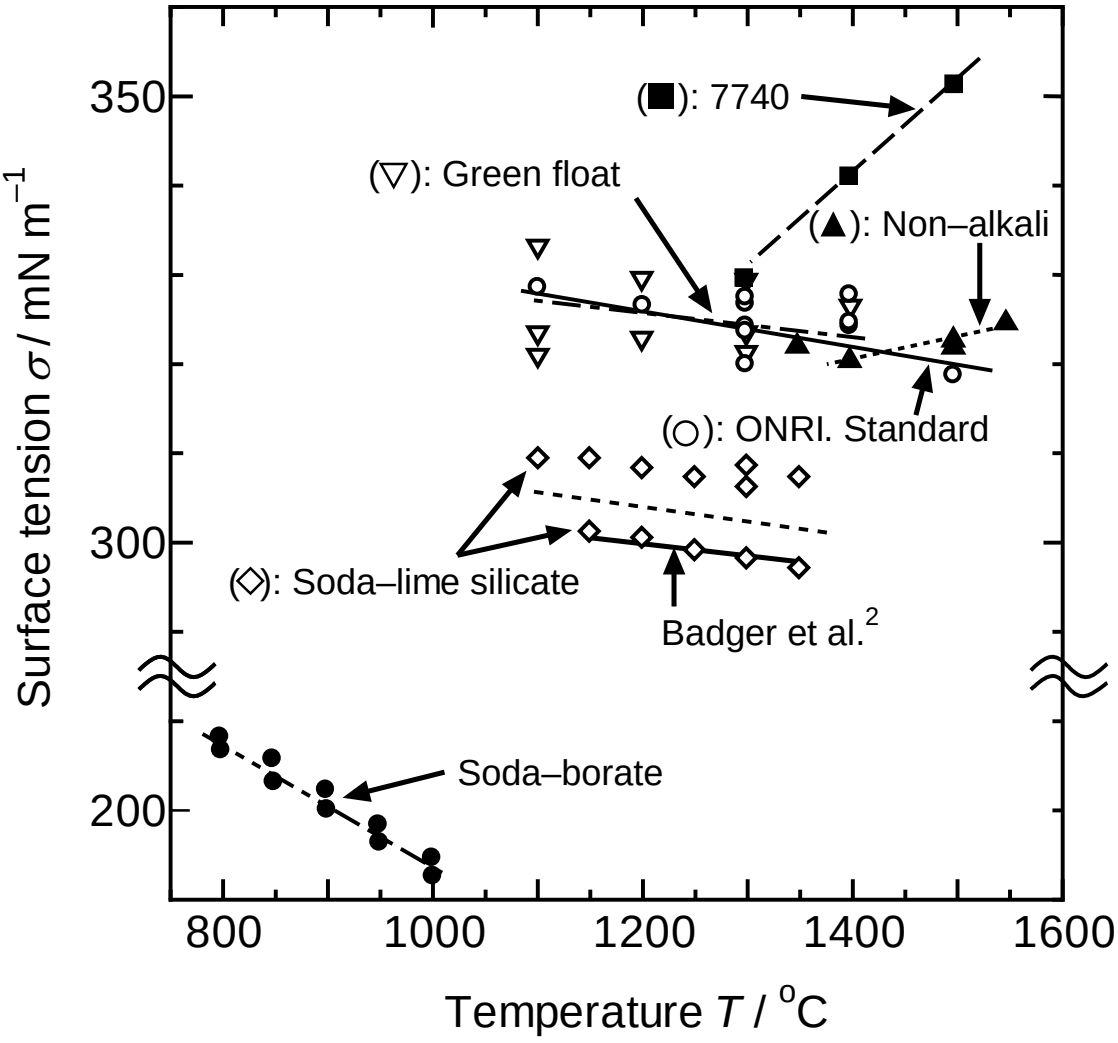

Fig. 11. Surface tension vs. temperature for several kinds of glass melts.

5-4 Discussion

5-4.1 *Accuracy and reproducibility of the static value*

There can be two kinds of experimental errors: statistical and systematic. In order to reduce statistical errors, the number of points in Region 1 should be large enough to obtain a reliable surface tension value. If the viscosity of the melt is high, the maximum bubble pressure values increase at high bubble-forming rates since the Stokes' force from viscosity, which is included in the pressure value, increases. Hence, Region 1 becomes narrow and it becomes difficult to obtain an accurate estimation of surface tension. To widen Region 1, tip (b) seems better than (a), as shown in Figs. 5 and 6, probably because tip (b) is less wettable by melt than tip (a); thus, capillary action, which increases the apparent σ value, could be suppressed on tip (b), which then results in a wider Region 1. Generally, however, a slower rate of bubble formation is needed to obtain an accurate value.

The measurement of the depth h of the edge of the tip from the surface of the melt also affects the error range under this method. The mechanical error limit of h was 0.3 mm, as mentioned above, which corresponds to 0.6% of the σ value. The volume of the tube dipped in the melt could be ignored in the present study, since the diameter ratio of the tube/crucible was 0.1, corresponding to only 0.05 mm in h when h was 5 mm. However, if the melt surface is depressed by the flow of the air, the error increases greatly. Thus, when determining the position of the tips, we stopped the air flow or lowered the air flow rate.

The error in the measurement of the tip hole radius r_0 was approximately ±2% since the hole was not a perfect circle and the edge was not very sharp. This error can cause a systematic deviation among tips. The discrepancy between the data values obtained with different tips, shown in Figs. 5 and 6 and summarized in Fig. 11, is

probably due to this deviation. The reproducibility of the values for each series of measurements was approximately 0.5%, as shown in Fig. 11.

Other errors could arise from the reading of P_{max}, the estimation of t_{max} etc. When the bubble grew slowly, the pressure occasionally fluctuated with time, probably because of pressure changes caused by slight fluctuations in temperature. This error would be of the same order as or less than the error in *h*.

The values of surface tension in the $20Na_2O$-10CaO-$70SiO_2$ glass melt shown in Fig. 11 were different from those reported in literature[2] about 0 and 3 %, respectively.

The viscosity of the 7740 melt was $10^{2.5}$ Pa·s at 1300°C, where the estimated error of extrapolation of the maximum pressure value to the zero bubble-forming rate was a few percent (Fig. 9). Below this level of viscosity, accuracy improved: in Fig. 9, it was probably within 1% at 1500°C. The accuracy of surface tension values for normal soda-lime silicate glass was ±2%, including systematic deviation. Hence, the maximum error for the 7740 melt at 1300°C is ±5%.

5-4.2 *Component factor*

The additive property applies to the composition of the glass in the case of surface tension as well as in other thermal properties. In silicate glass melts, surface tension factors for some components have been proposed on the basis of the additive properties,[10,19-22] and the surface tension can be calculated from the mol or mass fraction n_i and the factor *f* for each component using the equation

$$\sigma = \Sigma f_i \cdot n_i \,. \qquad (3)$$

Table 2 is a comparison of the values obtained in the present study and those calculated from Eq. (3) using the *f* values described in previous reports. The values agreed within ±5% for the three silicate melts.

Table 2. Comparison of surface tension values determined from various factors and experimental values in $mN \cdot m^{-1}$ at 1400 or 1200 ^{o}C. * The factor for SrO is assumed to be 5; and **, that for Fe_2O_3 is 4.5. The error ranges in the present study were estimated roughly from Figs. 1-3 and the experimental error discussed in the text. [ ] denotes extrapolated values.

	1400°C					1200°C	
	Present study (measured)	Kucuk et al.[10]	Lyon[19]	Boni and Derge[20]	Goleus et al.[21]	Present study (measured)	Rubenstein[22]
Soda-lime	300±5	305	296	320	306	304±5	300
ONRI. Std.	322±5	317	321	333	317	326±6	325
Green float	323±5	314	321	(333)**	(315)**	326±7	326
7740(Pyrex)	341±8	243	277	269	243	[320±12]	285
Non-alkali	321±5	331	(361)*	(351)*	322	[316±8]	367

However, for the two borosilicate melts, agreement was bad; the calculated value for 7740 was much smaller than our experimental result, and that for non-alkali glass was larger than the experimental value. For glasses with a higher or lower silica content than normal glass, the application of simple composition factors will cause error.[20] The non-alkali glass has a high alumina content and the $Al_2O_3 + B_2O_3$ amount exceeds the sum of MgO + CaO + SrO. When the amount of Al_2O_3 exceeds the amount of Na_2O in Na_2O-Al_2O_3-SiO_2 glass, some aluminum becomes a 6-coordinated state.[23] In the case of the non-alkali glass, there are two kinds of aluminum coordination which are similar to that find in the soda-aluminosilicate glass; they may be the cause of the discrepancy between the calculated and measured surface tension values.

Similarly, 7740 glass contains much more $Al_2O_3 + B_2O_3$ than network modifier elements such as alkalis and alkali earths, and the amount of B_2O_3 is much higher than that of Al_2O_3. In such a glass, there should be boroxol rings, and pentaborate, diborate[24] and silicon atoms which combine to form four bridging oxygen. There must be no non-bridging oxygen in this glass,[25] which differs from most glasses whose surface tensions have been measured to obtain the component factor *f*. However, not only this is the reason for the discrepancy since the factor for boron was found to be almost valid in a borosilicate glass with a much lower modifier content than B_2O_3 content.[26] The high SiO_2 content in 7740 would be responsible for the discrepancy. It is also possible that there may be some anomaly in the composition of the 7740; it is well known that its composition lies near the immiscible region.[27] In such a case, there may be some heterogeneity in the glass structure which affects the surface tension. Further study is needed to identify the reason.

5-5 Conclusion

The surface tensions of several glass melts were measured using the maximum bubble pressure method. Measuring error was decreased by suppressing capillary rise during bubble formation. Error was within a few percent in a viscose melt with $10^{2.5}$ Pa·s.

Surface tensions were also measured for several silicate melts and the obtained values were compared with values calculated based on empirical composition parameters which were previously reported. The 7740 borosilicate melt showed a large positive temperature dependence as well as a large discrepancy from the values calculated on the basis of the additive property. This suggests that the application of composition factors for surface tension is limited to normal glass composition and that

experimental evaluation is essential.

References

1. M. Cable, *J. Am. Ceram. Soc.*, **49**, 436-40 (1966).
2. A. E. Badger, C. W. Parmelee and A. E. Williams, *J. Am. Ceram. Soc.*, **20**, 325-329 (1937).
3. C. A. Bradley, *J. Am. Ceram. Soc.*, **21**, 339-344 (1938).
4. S. Akhtar and M. Cable, *Glass Technology*, **9**, 145-151 (1968).
5. A. Kucuk, A. G. Clare and L. E. Jones, *Proc. 18th Int. Congr. on Glass.* 1998. San Francisco, CA.
6. A. Kucuk, A. G. Clare and L. E. Jones, *Ceram. Trans.*, **82**, 287-298 (1998).
7. K. Ghanbari-Ahari, M. Askari and A. M. Cameron, *Phys. Chem. Glasses*, **32**, 72-76 (1991).
8. M. L. Huggins, *J. Am. Ceram. Soc.*, **26**, 4 (1943).
9. K. Takahashi, *Yogyo Kyokai-shi*, **63**, 142 (1955).
10. A. Kucuk, A. G. Clare and L. E. Jones, *Glass Technol.*, **40**, 149-153 (1999).
11. A. Yasumori, N. Nakazawa, D. Kawamura, Y. Kameshima and K. Okada, Abstract of 12th fall meeting of the Ceramic Society of Japan (1999) p.82.
12. K. Kubota, H. Masuda, S. Fujino and K. Morinaga, *J. Ceram. Soc. Japan*, **106**, 909-913 (1998).
13. M. Askari, A. M. Cameron and J. Oakley, *High Temp. Technol.*, **8**, 201-207 (1990).
14. S. Vaisburd and D. G. Brandon, *Meas. Sci. Technol.*, **8**, 822-826 (1997).
15. S. Sugden, *J. Chem. Soc.*, **1922**, 858-866 (1922).
16. H. Bloom, F. G. Davis and D. W. James, *Trans Faraday Soc.*, **56**, 1179 (1960).
17. V. B. Fainerman, A. V. Makievski and R. Miller, *Colloids Surf.*, **75**, 229-235 (1993).
18. G. Serrien and P. Joos, *J. Colloid Interface Sci.*, **139**, 149-159 (1990).

19. K. C. Lyon, *J. Am. Ceram. Soc.*, **27**, 186 (1944).

20. R. E. Boni and G. Derge, *J. Metals*, **8**, 53 (1956).

21. V. I. Goleus, A. Ya. Belyi, E. M. Sardak and Ya. I. Belyi, *Trans. Stek. Keram.*, **53**, 226 (1996).

22. C. Rubenstein, *Glass Technol.*, **5**, 36 (1964).

23. T. Hanada, T. Aikawa and N. Soga, *J. Non-Cryst. Solids*, **50**, 397 (1982).

24. P. J. Bray, In *Materials Science Research, Vol.12: Borate glass*. 1978. Ed. by L. D. Pye, V. D. Fréchette and N. J. Kreidl. Plenum Press, N.Y. Pp. 321-51.

25. W. L. Konijnendijk, *Philips Res. Repts. Suppl.*, **1**, (1975)., Pp. 81-122.

26. M. Imaoka, H. Hasegawa, Y. Hamaguchi and Y. Kurotaki, *Yogyo Kyokaishi*, **79**, 164 (1971).

27. W. Haller, D. H. Blackburn, F. E. Wagstaff and R. J. Charles, *J. Am. Ceram. Soc.*, **53**, 34 (1970).

Chapter 6. Solubility of noble metals in glass melts.

6-1 Introduction

Nuclear waste from spent nuclear fuel contains many elements. Though most of these elements are soluble in glass, platinum group metals are largely insoluble and precipitate at the bottom of the melt during the vitrification of nuclear waste. Since they can cause electrical shorting in a joule-heated ceramic melter, the glass melt is drawn out from the bottom of the melter together with the precipitates. In order to attain stable operation of the melter, it is necessary to characterize the behavior of platinum group metals. Among these metals, the behavior of ruthenium is most important since ruthenium content is the highest and unlike rhodium or palladium, which exist as metals or tellurides, ruthenium exists as oxides, which possess high electrical conductivity. Krause et al.[1] reported in detail on the behavior of these metals and concluded that needle-shaped RuO_2 crystals, which affect conductivity and viscosity, were formed by gas-phase reaction in voids between glass beads before complete melting.

Dissolution of ruthenium in silicate glass and resulting changes in coloration have been reported by Mukerji et al.[2-5] According to these studies, ruthenium solubility depends on glass composition and melting temperature, and is more than 0.1 mass% at 1400 ^{o}C in ordinary soda-silicate glass. On the other hand, Schreiber et al.[6] reported that ruthenium solubility in soda-lime silicate glass was below 0.001 mass% at 1150 ^{o}C and coloration was not observed. The amount of RuO_2 they used was far greater than that of expected solubility; we wondered whether that had an effect on the results.

In the present study, dissolution and coloration of ruthenium was investigated in aluminoborosilicate glass used for nuclear waste solidification. The effect of the RuO_2 amount added in the melt was examined, in addition to the effects of various melting/heating and cooling regimens.

6-2 Experimental

The composition of the chosen base glass was $58.4SiO_2$-$7.7Na_2O$-$7.6Li_2O$-$15.7B_2O_3$-$4.0CaO$-$3.7Al_2O_3$-$2.8ZnO$ in mol%. Raw materials as carbonates or hydroxides were mixed thoroughly and melted at 1200 ^oC in a platinum crucible in an electric furnace, then cast and crushed to powder. An appropriate amount of ruthenium was added to 40 g of the glass powder as ruthenium dioxide (RuO_2, 99.9%, Soekawa Rikagaku) or ruthenium nitrosyl nitrate ($Ru(NO)(NO_3)_3 \cdot nH_2O$, Alfa Aesar, Ward Hill) aqueous solution. The mixture was remelted at 1200^o to 1400^{o}C in an alumina crucible (SSA-S, Nikkato) with a lid to avoid volatilization of ruthenium tetroxide. The lid was kept securely on the crucible throughout the experiment to prevent ruthenium loss due to volatilization. Melting time was usually 2 hours. The melt was slowly cooled in the crucible, cast by pouring onto a graphite plate or quenched in water. The cast and quenched samples were annealed at 550 ^oC. The obtained glass sample containing 0.2 mass% of RuO_2 that was added as $Ru(NO)(NO_3)_3 \cdot nH_2O$ was analyzed by X-ray fluorescence (System 3370, Rigaku, Akishima, Japan) to confirm there had been no serious loss of ruthenium due to volatilization. All specimens of the glass were crushed, ground and then thoroughly mixed. This sample was compared with glass powder containing ruthenium before remelting and 100 + 2% of ruthenium was detected.

Each sample was cut to a thickness of 2 mm, then ground and polished to give two flat and parallel faces. Optical absorption spectra were measured with a spectrophotometer (U-4000, Hitachi). The interiors of the samples were observed with an optical microscope (BHM, Olympus). The effect of addition of Mo in glass was also tested and the crystal shape of RuO_2 was observed.

The ruthenium ion contents in the quenched samples were analyzed by wet method as described by Mukerji et al.[2] After decomposition of samples with HF

Table 1. Ruthenium ion content in glasses melted at 1400 °C and quenched, as measured by wet analysis.

Sample No.	RuO_2 content (mass%)	Ru ion amount (mass% as RuO_2)
A	0.02	0.011
B	0.03	0.018
C	0.05	0.025
D	0.1	0.024

solution, evaporation and drying were conducted under Ar atmosphere. Instead of dithio-oxamide, thiourea was used for spectrophotometric analysis.[7] Absorption spectra were measured in the range of 200 to 1000 nm and the absorbance at 640 nm was used for the analysis.

6-3 Results and Discussion

All glasses melted at 1400 °C and quenched turned light yellow to greenish yellow. Figure 1 shows spectra of ruthenium-containing quenched glasses. Absorptions at 700 nm and below 500 nm were assigned to Ru^{4+}.[4] Black dispersed precipitates were apparent with the addition of more than 0.05 mass% of RuO_2. They were identified as RuO_2 by X-ray diffraction. Table 1 shows results of ruthenium ion contents by wet analysis. Glasses containing 0.05 or 0.1 mass% of RuO_2 showed the same ruthenium contents: This 0.025 mass% should be the solubility in this glass at 1400 °C: if glasses were saturated with ruthenium ion, the analyzed concentration would be identical if the content exceeded the saturated value. The values in Table 1 imply that dissolution of

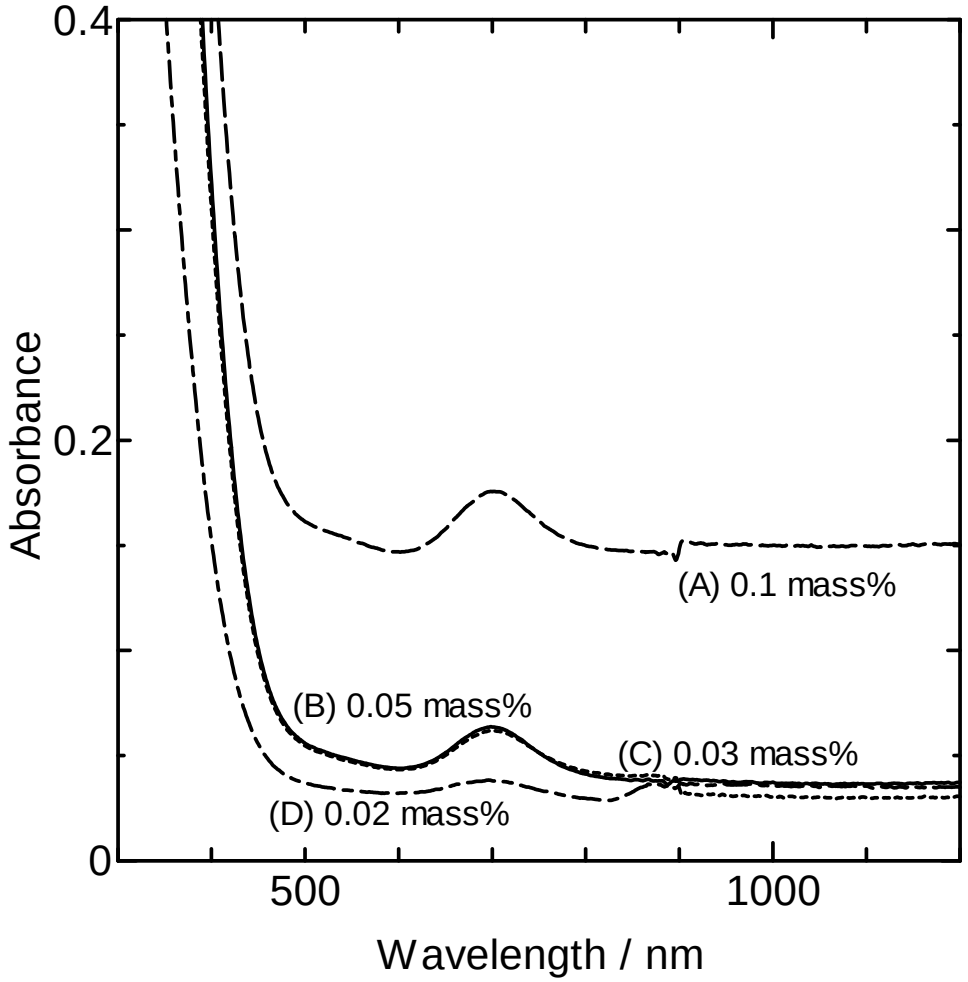

Fig. 1. Optical absorption spectra of RuO_2-containing glasses melted at 1400 ^oC and quenched in water. RuO_2 content: 0.1 mass% for dashed line (A), 0.05 for solid line (B), 0.03 for dotted line (C) and 0.02 for dotted and dashed line (D). Y-axis shows absorbance per 1 mm thickness. A discontinuity at 900 nm was caused due to automatic switching of the detector.

ruthenium is incomplete with melting for 2 hours if the RuO_2 content is not high. As shown below, the dissolved amount becomes smaller at lower temperatures. Ruthenium ion contents in Table 1 were not proportional to peak heights at 700nm on spectra in Fig. 1. For example, glasses (B) and (C), which contained 0.05 and 0.03 mass% of RuO_2, respectively, showed almost the same spectra though the values in Table 1 differed. Two explanations are possible. One is that the valence state of ruthenium ions changed. Though comparison of spectra in Fig. 1 and Ru^{4+} spectrum measured by Mukerji et al.[4] indicates that most ruthenium ions in the melt must be Ru^{4+}, valence change of small amount of ruthenium might alter the peak height. The other possibility is colloidal formation during annealing. When the quenched glass having greenish yellow color was heated above 600 ^{o}C, it turned dark green with a temperature raise. The spectrum was changed as follows: at first, the peak at 700nm became high at 600 ^{o}C; above 700 ^{o}C, the absorbance raised for all wavelengths except for that around 600 nm. This spectral change may be attributed to RuO_2 colloids. If such spectral changes occurred, the peak heights at 700 nm in spectra would not be proportional to the Ru^{4+} content.

The 0.05 mass% RuO_2 glass that was melted at 1400 ^{o}C and slowly cooled showed a yellowish color with green sediment. The sediment showed the same spectrum as the quenched glass annealed above 700 ^{o}C. When glasses contained more than 0.1 mass% of RuO_2, slow-cooled samples containing large amounts of dispersed precipitations were a colorless gray. Figure 2 shows the effect of cooling rates on absorption spectra in glasses containing 0.1 mass% of RuO_2. Quenched and cast samples showed a greenish yellow color accompanied with RuO_2 precipitation. The slow-cooled sample had no clear absorption at 400 nm. In a glass containing 0.5 mass% of RuO_2, the tendency was the same. In slowly cooled glass, most RuO_2 existed as

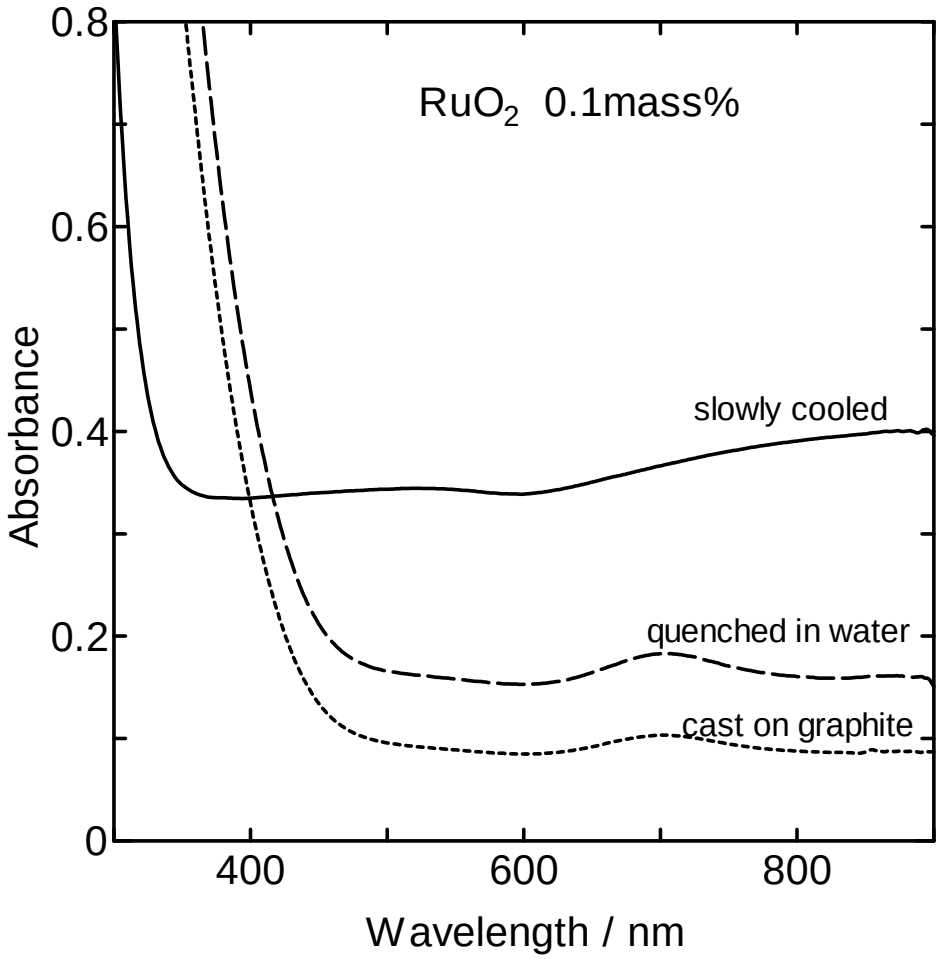

Fig. 2. Changes in absorption spectra with different quenching rates for glass containing 0.1 mass% of RuO_2 melted at 1400 ^{o}C.

aggregations of irregularly shaped crystals; considerably fewer of them were needle-shaped, and those were shorter, at a length of 10 μm or less. Since ruthenium ion must be in a supersaturated state during cooling, these occurrences indicate that a large excess of ruthenium, which exists as RuO_2 particles in the melt, accelerates the precipitation of dissolved ruthenium during cooling.

At 1200 ^oC, glass coloration due to ruthenium was not observed. The shape of RuO_2 crystals after vitrification was determined by the shape of crystals in the added glass powder, which is to say that the addition of fine RuO_2 powder produced much dispersed precipitation. When $Ru(NO)(NO_3)_3 \cdot nH_2O$ aqueous solution was added, crystal shape was determined by the shape of the crystals therein following dehydration and denitration at a maximum of 400 ^oC. The aggregated crystals formed by denitration were unchanged at melting temperatures. The black ones were dispersed in colorless transparent glass. The addition of MoO_3, which has been said to produce needle-shaped crystals,[1] did not accelerate the formation of needle-shaped crystals at 1200 ^oC.

When the glass containing 0.05 mass% of RuO_2 was melted at 1400 ^oC and kept at 1200 ^oC for 1 or 12 h, the yellowish color became pale, as shown in Fig. 3, and the dispersed black precipitate increased. This means that a certain amount of time is required for separation of RuO_2 to occur when the amount of ruthenium is not excessive. Many needle-shaped crystals were observed in this glass by microscopic observation as shown in Fig. 4. From these facts, it is concluded that needle-shaped crystals are formed in the melt by slow growth from separation of dissolved ruthenium during slow cooling.

6-4 Conclusion

The solubility of ruthenium in borosilicate glass for the immobilization of

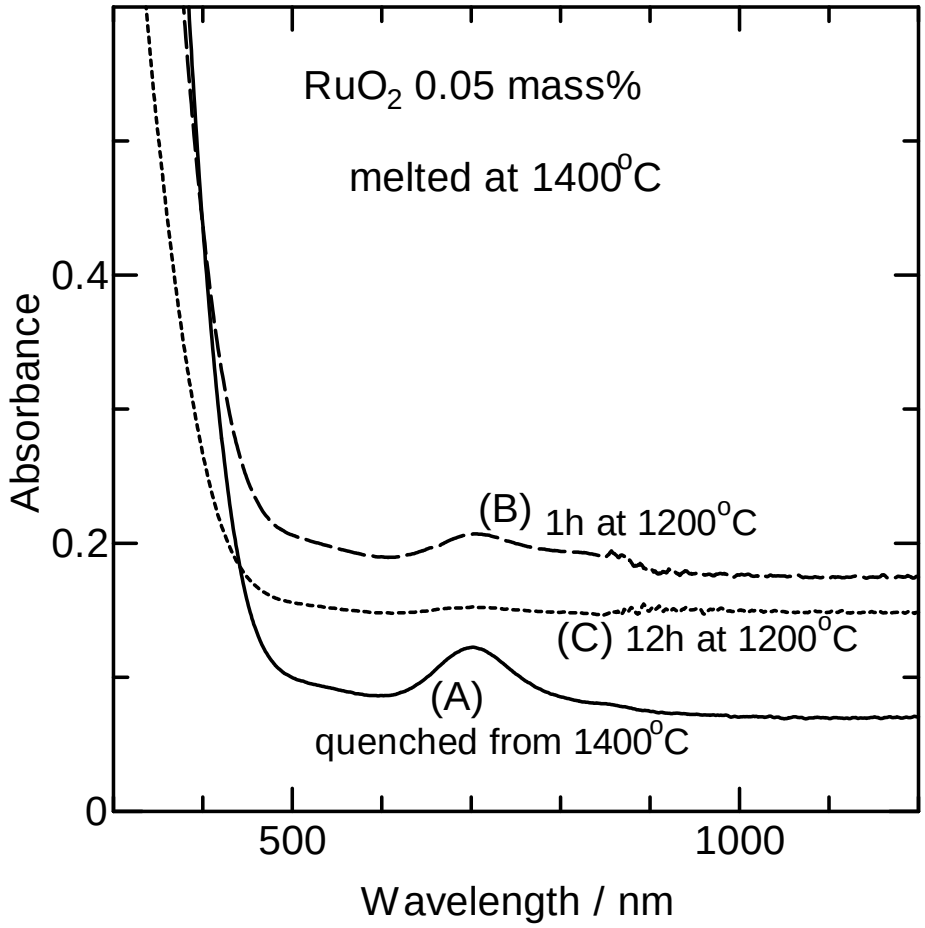

Fig. 3. Changes in absorption spectra with heat treatment at 1200 °C for glasses containing 0.05 mass% of RuO_2 melted at 1400 °C. Sample (A) received no heat treatment and samples (B) and (C) successively heated for 1 and 12 h, respectively, following melting at 1400 °C. All glasses were quenched in water.

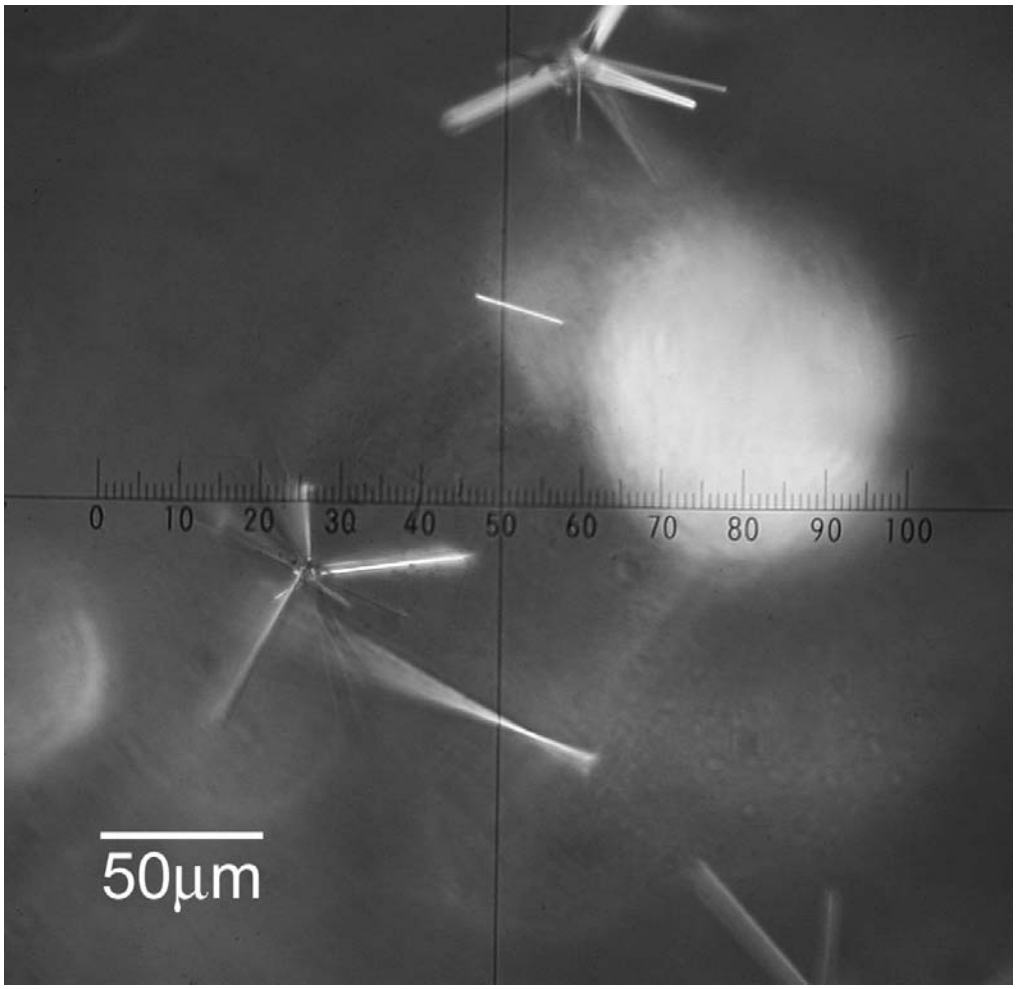

Fig. 4. Needle-shaped RuO_2 crystals seen in sample (B) in Fig. 3.

nuclear waste was examined and the following results were obtained. At 1400 ^{o}C, ruthenium dissolved as +4 ions, the amount of which was about 0.025 mass% as RuO_2. An excess amount of RuO_2 was separated and dispersed in glass. Excessive addition of ruthenium (more than 3 times the solubility) accelerates separation of ruthenium ion during cooling and produces colorless glass. At 1200 ^{o}C, dissolved ruthenium was not optically detectable.

RuO_2 crystal shape was observed with an optical microscope and was found to be unchanged by melting at 1200 ^{o}C. While it is not the intent of this study to deny the formation of needle-shaped crystals in the cold cap, at least a portion of these crystals were formed by a dissolution-separation mechanism when slow cooling was performed.

References

1. Ch. Krause and B. Luckscheiter, *Mater. Res.*, **6**, 2535-2546 (1991).
2. J. Mukerji and S. R. Biswas, *Cent. Glass Ceram. Res. Inst. Bull.*, **14**, 30-34 (1967).
3. S. R. Biswas and J. Mukerji, *Cent. Glass Ceram. Res. Inst. Bull.*, **15**, 99-103 (1968).
4. J. Mukerji and S. R. Biswas, *Glass Technol.*, **12**, 107-111 (1971).
5. J. Mukerji, *Glass Technol.*, **13**, 135-137 (1972).
6. H. D. Schreiber, F. A. Settle, Jr., P. L. Jamison, J. P. Eckenrode and G. W. Headley, *J. Less-Common Metals*, **115**, 145-154 (1986).
7. G. H. Ayres and F. Young, *Anal. Chem.*, **22**, 1277-1280 (1950).